

Multivariate chemo-rheological framework for optimizing laboratory aging protocols of paving binders

Khalighi, Sadaf; Ma, Lili; Mosleh, Yasmine; van Lent, Diederik; Varveri, Aikaterini

DOI

[10.1016/j.matdes.2024.113520](https://doi.org/10.1016/j.matdes.2024.113520)

Publication date

2024

Document Version

Final published version

Published in

Materials and Design

Citation (APA)

Khalighi, S., Ma, L., Mosleh, Y., van Lent, D., & Varveri, A. (2024). Multivariate chemo-rheological framework for optimizing laboratory aging protocols of paving binders. *Materials and Design*, 248, Article 113520. <https://doi.org/10.1016/j.matdes.2024.113520>

Important note

To cite this publication, please use the final published version (if applicable). Please check the document version above.

Copyright

Other than for strictly personal use, it is not permitted to download, forward or distribute the text or part of it, without the consent of the author(s) and/or copyright holder(s), unless the work is under an open content license such as Creative Commons.

Takedown policy

Please contact us and provide details if you believe this document breaches copyrights. We will remove access to the work immediately and investigate your claim.



Multivariate chemo-rheological framework for optimizing laboratory aging protocols of paving binders

Sadaf Khalighi^{a,*}, Lili Ma^a, Yasmine Mosleh^a, Diederik van Lent^b, Aikaterini Varveri^a

^a Delft University of Technology, Stevinweg 1, 2628 CN Delft, the Netherlands

^b Netherlands Organizations for Applied Scientific Research (TNO), Van Mourik Broekmanweg 6, 2628 XE Delft, the Netherlands

ARTICLE INFO

Keywords:

Laboratory accelerated aging
Field aging
Multivariate analysis
MLR
PCA
SVR

ABSTRACT

This study aims to improve laboratory aging procedures for bituminous materials to better replicate field conditions. Two binders and mixtures were subjected to various levels of humidity, temperatures, pressures, film thicknesses, and aging durations. By comparing these lab-aged samples to field-aged samples, the study aims to simulate real-world aging more accurately. Fourier-transform infrared (FTIR) spectroscopy and frequency sweep tests were employed to analyse these samples. Multivariate techniques—Principal Component Analysis (PCA), Multiple Linear Regression (MLR), and Support Vector Regression (SVR)—were used to explore chemical and rheological relationships, evaluate the interchangeability of aging factors, and quantify the equivalency between laboratory and field aging. The findings revealed that increased temperature, pressure, and duration lead to more oxidative products. The PCA distinguished between two binders and aging trends, highlighting the importance of both FTIR and rheological measurements. The SVR model demonstrated strong predictive performance for rheological properties, identifying critical FTIR region, 710–912 ⁻¹cm. By MLR model, optimal aging conditions to simulate nine years of field aging for porous asphalt and stone mastic asphalt were back-calculated. The Euclidean distance found laboratory conditions that closely match field-aged samples. SVR models provided predictions of simulated field aging time for various laboratory aging conditions.

1. Introduction

Bituminous binder, an organic material characterized by its heterogeneous composition and viscoelastic properties, serves a pivotal role in road construction applications [1,2]. Binder must adhere to specific standards, typically relating to its physical, particularly rheological, properties, to ensure optimal performance and durability of asphalt pavements [3]. However, the hydrocarbon nature of binder makes it susceptible to environmental aging factors, which increases the risk of pavement damage, particularly cracking [4]. This degradation occurs in two separate phases: short-term aging (STA) and long-term aging (LTA) [5]. Processes like the evaporation of volatile components, steric hindrance, and oxidation play a role in the aging of bitumen during these stages. Oxidative aging, in particular, significantly impacts the long-term performance of pavements. To ensure optimal performance and durability of asphalt pavements, it is essential to evaluate binder performance under the laboratory aging procedures that can accurately simulate field aging conditions [2].

Short-term aging (STA) occurs primarily during production, mixing,

transportation, and construction of the asphalt mixture [5]. In this phase, elevated temperatures are typically employed to facilitate mixing, which leads to rapid oxidation and the loss of volatile components from the binder. These effects, compounded by exposure to high temperatures for relatively short durations, result in an initial hardening of the binder, influencing its immediate properties and workability during pavement construction [5,6]. The Rolling Thin Film Oven (RTFO) and Thin Film Oven (TFO) protocols are the standard methods used to simulate STA in the laboratory setting. The RTFO method subjects binder films to a controlled air flow at 163 °C for 75 min, while the TFO ages binder films of 3.2 mm thickness at the same temperature but for 5 h [7].

Long-term aging (LTA), on the other hand, occurs gradually over the pavement's service life under environmental conditions that promote ongoing oxidative aging and further hardening of the binder. Unlike STA, which is primarily temperature-dependent, LTA is influenced by a combination of factors, including temperature, pressure, and prolonged exposure to oxygen. Laboratory simulation of LTA is typically achieved using the Pressure Aging Vessel (PAV) method, which ages 3.2 mm

* Corresponding author.

E-mail address: s.khalighi@tudelft.nl (S. Khalighi).

<https://doi.org/10.1016/j.matdes.2024.113520>

Received 18 October 2024; Received in revised form 20 November 2024; Accepted 1 December 2024

Available online 5 December 2024

0264-1275/© 2024 The Author(s). Published by Elsevier Ltd. This is an open access article under the CC BY-NC license (<http://creativecommons.org/licenses/by-nc/4.0/>).

binder films in a pressurized vessel with air at 2.07 MPa and temperatures ranging from 90 to 110 °C for 20 h [8]. This method attempts to replicate the oxidative conditions the binder experiences over years in the field, accounting for environmental stressors that progressively alter binder properties. For asphalt mixtures, long-term aging is commonly simulated using extended oven aging and pressure oxidation. The SHRP method involves aging compacted specimens at 85 °C for 5 days [9], whereas pressure oxidation utilizes a low-pressure oxidation technique in a forced draft oven with an oxygen flow rate of 1.9 L/min at 85 °C for the same duration [10]. In this study, the primary focus is on long-term aging, with particular attention to the effect of different aging parameters—such as temperature, pressure, and exposure time—on the binder's rheological and chemical properties.

However, several studies emphasize the challenges in precisely reproducing field conditions and predicting the natural aging of pavements using the above mentioned methods [5]. Discrepancies between samples aged in the laboratory and those aged in the field are addressed in existing literature sources [10–20]. Variations between laboratory and field-aged samples can occur due to the absence of environmental aging factors in laboratory procedures. Binder undergoes aging in real-world conditions where it is exposed to moisture, temperature variations, and traffic factors that are often overlooked in standard aging protocols. A comprehensive aging protocol should incorporate these elements and accelerate their effects to mimic field aging accurately. Before integrating these factors, it is crucial to comprehend their individual impacts. This study examines the influence of temperature, pressure, binder thickness, moisture, and time on bituminous binder aging in binder and mixture levels.

Temperature plays a critical role in the aging of bituminous binders, as oxidation reactions in binders proceed more rapidly at higher temperatures. Many aging protocols, such as the PAV method, use elevated temperatures to simulate aging; however, these are typically higher than temperatures experienced by pavements during their service life. Elevated temperatures not only accelerate the rate of reaction but can also influence the pathways of the reaction, deviating from natural field aging, particularly at temperatures exceeding 90–100 °C [5]. In the Netherlands, maximum air temperatures generally reach only 30–35 °C [21]. Though pavement temperatures are not commonly measured directly, they are known to exceed air temperatures by 27–50 °C on sunny days, which implies potential pavement surface temperatures between 60 °C and 85 °C [22]. The upper temperature of 85 °C chosen for this study accounts for this air-pavement temperature difference, making it suitable not only for the Netherlands but also for regions with higher average temperatures [23]. Moreover, several recent long-term aging protocols have adopted similar maximum temperatures, such as 80 °C, to maintain reaction pathways that closely mimic natural field aging while accelerating aging rates [10,24]. Other protocols, by contrast, use a lower temperature, around 60 °C, to avoid excessive reaction deviations [10,25]. Consequently, this study examines temperatures of 60 °C, 70 °C, and 85 °C to provide a comprehensive range that balances accelerated oxidation rates with realistic field-like conditions and includes an intermediate temperature for a nuanced understanding of aging progression [21].

In addition to temperature, pressure also plays a role in influencing the aging reaction of binder. This is because pressure enhances the diffusion rate of oxygen in the binder, leading to a higher rate of oxidation reaction [21]. Previous studies commonly utilize 20 bar as the upper limit for pressure in binder aging experiments. To assess the necessity of applying such high pressure, this study examines other pressures, including 5 and 10 bar. Furthermore, an exceptionally high pressure of 150 bar is included to investigate the accelerated impact of pressures exceeding 20 bar.

Selecting an appropriate binder film thickness is a critical aspect of developing an effective aging protocol. In actual pavement structures, binder film thickness varies significantly, ranging from approximately 100 to 700 µm around large aggregates and 9 to 100 µm around filler

particles [26–28]. Research on polymer-modified mixtures indicates that binder films that are too thin compromise aggregate bonding and overall pavement performance, while excessive thickness reduces mixture stiffness and lowers resistance to cracking and fatigue under load [29]. However, replicating submicron thicknesses in the lab is challenging, as factors like substrate and application method influence film uniformity and aging behaviour. To develop a practical aging protocol, it is necessary to select a film thickness that realistically represents the binder thickness in actual pavements, while also being feasible to produce consistently with standard laboratory equipment. Importantly, the chosen thickness should allow sufficient material for post-aging rheological and chemical characterization. Various studies have demonstrated that changes in film thickness lead to different aging effects [10]. For instance, studies have shown that reducing film thickness from 3.2 mm to 1 mm leads to a significant increase in oxidized molecules, as well as higher complex shear modulus and lower phase angle after aging, indicating increased stiffness and reduced viscoelasticity [30]. Different binder aging protocols utilize specific film thicknesses based on these considerations. For example, the Viennese Binder Aging (VBA) protocol employs a film thickness of 0.5 mm to enhance aging efficiency [24], while the widely-used Pressure Aging Vessel (PAV) protocol typically employs a 3.2 mm film thickness [30]. However, the authors' own experience has shown that producing consistent 0.5 mm films in petri dishes is time-consuming and challenging. Consequently, this study evaluates a range of thicknesses, beginning with 1 mm and extending to 3.2 mm, with an intermediate thickness of 2 mm. This range was selected to examine how varying film thickness influences aging behaviour and to identify a practical balance between accelerated aging effects and experimental feasibility. By assessing thicknesses of 1, 2, and 3.2 mm, this study aims to develop an optimized protocol that maximizes relevance to field conditions while ensuring sufficient material is available for detailed characterization post-aging.

Moisture plays a crucial role in binder aging protocols due to its significant impact on binder properties and asphalt performance. Molecular dynamic simulations have revealed that increased moisture content leads to various detrimental effects on binder, such as reduced density, glass transition temperature, viscosity, and cohesive energy [31]. Furthermore, it was shown experimentally that hygrothermal aging can accelerate aging processes in bituminous binders compared to thermo-oxidative aging [32]. Despite some studies indicating minimal influence of moisture on binder aging or variations among binder types [33], further research is necessary to fully understand the specific effects of moisture and develop more accurate aging protocols. Hence, this study examines how the presence of humidity during aging, at various temperatures and pressures, affects binder, considering different thicknesses and types of binders.

The final crucial aging factor investigated in laboratory protocols is time. As aging duration increases, more pronounced aging effects become evident in the binder properties [5]. However, selecting the appropriate aging duration requires a reference sample to determine the desired level of aging. Additionally, the aging duration should align with industrial requirements, avoiding excessively long durations. Therefore, this study employed field-aged samples aged for 9 years as a benchmark to devise a duration for simulating 9 years of field aging. The binder was subjected to aging in a PAV for durations ranging from 5 to 80 h.

Other aging factors such as atmospheric ROS, including ozone (O₃) and nitrogen oxides (NO_x), significantly contribute to binder aging under ambient conditions [34,35]. The Viennese Binder Aging (VBA) method, which enriches air with O₃ and NO_x, has shown NO₂ induces significant aging, while O₃ has milder effects [24,36,37]. Moreover, UV radiation also causes chemical changes in binders, particularly in the 300–350 nm range [38,39]. However, UV aging is shallow due to the formation of an impermeable surface layer over time, limiting oxygen penetration [40,41]. While these factors are critical, their inclusion requires specialized equipment, which will be a focus of future studies.

Multivariate analysis has been broadly used to uncover complex

relationships between various parameters, leading to more informed decisions in pavement engineering and material selection. In the field of pavement engineering, Siroma et al. [42] exclusively employed phase angle master curves and multivariate statistical methods, like principal component analysis (PCA) and hierarchical cluster analysis (HCA), to determine the aging status of binder samples. In another study by Ma et al., PCA-linear discriminant analysis (LDA) on FTIR spectra was utilized. The study classified different types of binder at various aging stages, highlighting key chemical differences necessary for accurate classification. Aliphatic and aromatic bonds in the spectrum were important for identifying binder types, with notable chemical changes seen in the 1800–900 cm^{-1} range [43]. In a study by Primerano et al., they aimed to distinguish between light, PAV, and VBA aged samples based on original FTIR spectra. To achieve this, they applied multivariate analysis utilizing random forest, PCA, and partial least squares discriminant analysis (PLSDA) methods. The study identified crucial wavenumbers for efficient classification of samples at different aging conditions [44]. Except using chemical or rheological parameter separately, Khalighi et al. used both chemical indices and rheological indices to compare lab-aged samples with field-aged samples using HCA [32]. Weigel and Stephan [45] used the FTIR spectra and its first derivative to feed the LDA and PLS regression algorithms, showing that despite varying grades and aging states, bituminous binder samples could be well-distinguished based on the refinery. Moreover, in another study by Weigel and Stephan [46], the calculated FTIR peak areas were used to create PLS regression models for describing and predicting different bituminous binder parameters such as penetration, complex shear modulus, phase angle, and asphaltene content. In the work of Ma [47], the PCA-LDA modelling was applied to the pre-processed FTIR datasets to differentiate among binder types, laboratory aging states, and lab/field conditions. Moreover, the FTIR datasets utilized for predicting rheological properties by PLS and Support Vector Regression (SVR). Comparing PLS and Support Vector regression, the conclusion in this thesis was that the prediction accuracy of SVR model is higher than PLS perhaps due to its ability to capture better the inherent nonlinear chemical-rheological relationship of bituminous binders, which can be achieved through the use of various kernel functions. To optimize binder aging protocols, multivariate analysis was used to provide a comprehensive understanding of the aging process. By analysing both chemical and rheological data simultaneously, multivariate methods offered a holistic approach to characterize binder properties. These techniques allowed for the identification of key chemical changes and rheological behaviours associated with different aging conditions, facilitating the development of accurate aging protocols.

2. Objective

The aim of this research is to develop more precise laboratory aging protocols for bituminous materials to better simulate their field aging process. Moreover, this research aims to develop a comprehensive chemo-mechanical analysis of the aging process in bituminous materials using multivariate techniques, focusing on pinpointing laboratory-aged samples that closely match field-aged samples.

The experiment framework examines the impact of combined moisture (0 and 99 % environment relative humidity), temperature (60, 70, 85 °C), pressure (5, 10, 20, 150 bar), film thickness (1, 2, 3.2 mm), and aging time (5, 10, 20, 40, and 80 h) on two binders from different sources (Q and T binder), along with two Q-mixture types, namely porous asphalt (PA) and stone mastic asphalt (SMA). The unmodified binder, which had undergone short-term aging, was subjected to long-term aging with the abovementioned conditions. To characterize the aged binder samples, Fourier-transform infrared (FTIR) spectroscopy and frequency sweep test were conducted.

The multivariate analysis objectives are structured as follows:

First, for chemical-rheological analysis, PCA was initially utilized to group all samples based on binder type and ageing impact using both

chemical and rheological parameters. The critical chemical and rheological parameters contributing to the differentiation of ageing was then identified utilizing the PCA results.

Second, SVR was applied to understand the relationship between chemical and rheological properties by correlating each rheological parameter with all the chemical parameters.

Third, MLR was employed to analyse the relationships between independent variables (temperature, pressure, and time) and to estimate the aging levels of samples based on FTIR and DSR results. The goal is to determine how each factor uniquely or interactively influences the aging process. The model further will be used to back-calculate the aging conditions that simulate nine years of field aging for porous and stone mastic asphalt.

Fourth, for comparing laboratory and field aging PCA-based distances were used to compare laboratory-aged samples with field-aged samples, identifying which laboratory aging conditions closely resemble the field-aged ones.

Finally, SVR was implemented to train a model based on field data, predicting the equivalent years of field aging for various laboratory aging conditions. This helps establish a direct comparison between laboratory procedures and actual field aging.

These five steps aim to ultimately develop laboratory aging procedures that more accurately mimic natural field aging, enhancing the reliability of laboratory tests in predicting the long-term performance of bituminous materials in real-world conditions.

3. Materials and methods

3.1. Materials and samples preparation

3.1.1. Materials

Binder PEN 70/100 is one of the most used bituminous binders for road construction in the Netherlands. In this study, two PEN 70/100 bituminous binders from two different suppliers (namely Q and Total) and thus from different crude oil sources were evaluated, named as Q and T, respectively. Table 1 shows the basic properties of the binders.

3.1.2. Samples preparation

To prepare binder samples, 50 g of fresh binder were poured onto pans which yielded films of 3.2 mm in thickness. These pans were subjected to short-term aging using oven aging at a temperature of 163 °C for 5 h, in line with the EN 12607-2 [1] standard. Specific amounts of short-term aged binders were then poured onto glass petri-dishes to achieve the desired thicknesses of 1, 2, and 3.2 mm. Uniformity of the binder films was achieved by placing all petri-dishes in an oven at a temperature of 163 °C for 3 min. The entire process of sample preparation and aging is graphically depicted in Fig. 1S.

For the mixture samples, asphalt slabs were prepared using Norwegian sandstone, with a nominal maximum size of 16 mm (density 2740 kg/m^3), and Q binder (Q-mixtures). The target air void contents were 16

Table 1
Properties of Q 70/100 and T 70/100 in fresh (unaged) state.

Property	Unit	Q PEN 70/ 100	T PEN 70/ 100
Penetration at 25 °C	0.1 mm	70–100	70–100
Softening point	°C	43–51	43–51
Complex shear modulus at 1.6 Hz & 60 °C	kPa	1.8	2.3
Phase angle at 1.6 Hz & 60 °C	°	88	88
Elemental composition	Nitrogen N (%)	0.59	0.93
	Carbon C	79.19	87.23
	Hydrogen	10.81	11.26
	H	4.47	3.35
	Sulfur S	2.25	0.60
	Oxygen O		

% and 5 % for the PA and SMA mixtures, respectively. The binder contents were 5.0 % and 6.4 % for the PA and the SMA mixtures, respectively. The mixture composition and grading details are outlined in Table 1S.

After the artificial aging in the lab, the binders from all the various aged asphalt mixture cores were extracted according to NEN-EN 12697-1:2012. The cold extraction method was used, where the binder was dissolved using dichloromethane. The binder was recovered from the dichloromethane by means of a rotary evaporator following the European standard (EN 12697-3:2013).

3.1.3. Aging conditions

The binder samples were tested at three states: unaged binder (fresh), short-term ageing (STA), and long-term ageing (LTA). For LTA, short-term aged binder underwent PAV treatment at varied conditions: temperatures (60, 70, 85 °C), pressures (1, 5, 10, 20 bar), durations (5, 10, 20 h), humidity levels (0 and 99 % RH), and thicknesses (1, 2, 3.2 mm), across two binder types (Q and T) and two Q-mixture types (PA and SMA). Additionally, the impact of extended hygrothermal aging was examined by subjecting 1 mm binder films to prolonged exposure under hygrothermal conditions for 40 and 80 h. To introduce humidity into the Pressure Aging Vessel (PAV), a quantity of 1000 g of demineralized water at room temperature was utilized to create > 99 % relative humidity via evaporation (Fig. 2S). Further information regarding the humidity measurement in the PAV chamber can be found in the [supporting information](#). To study the effect of extreme pressure, a custom-built oven was employed to elevate the pressure within the aging environment to 150 bar. This chamber facilitated the investigation of the exceptionally high pressures effects on the aging characteristics of both binders and mixtures. Notably, due to limitations, moisture could not be introduced to this chamber, thereby restricting the experiment to thermo-oxidative conditions. Table 2 presents all testing conditions.

3.1.4. Nomenclature

In this study, the nomenclature of samples is based on their binder/mixture type and the specific aging conditions applied. The fresh and short-term aged binder samples are labelled as F and STA, respectively. The designation of long-term aged binder samples adheres to a consistent framework, presented in Fig. 1a. This naming structure comprises five segments. The initial part designates the binder type, either Q or T. Subsequently, the letter “L” signifies long-term aging, followed by either “D” (representing dry, i.e., thermo-oxidative) or “W” (indicating wet, i.e., hygro-thermal) aging conditions. The fourth part contains information about the specific aging variables, with temperature, pressure, and time, signified by their units, denoted as C (Celsius), B (Bar), and H (Hours), respectively. Notably, this experiment maintains one variable while the rest remain fixed, as explained in Table 2. For instance, the inclusion of “85C” in the name implies that temperature serves as the varying factor, with pressure and time remaining constant at 20 bar and 20 h, respectively. The final section denotes the thickness of the binder films, which may take values of 1, 2, or 3.2 mm. In the case of 3.2 mm films, the value “3” was adopted for simplicity in the naming scheme. Fig. 1b illustrates the nomenclature format used for mixture samples. This format comprises three components: the type of mixture (PA for

porous asphalt or SMA for stone mastic asphalt), the presence or absence of humidity during aging (indicated by W or D), and the temperature applied. Similar to the approach seen in Fig. 1a, one factor is varied while other parameters are held constant, as demonstrated in Fig. 1b.

3.2. Characterization

3.2.1. Attenuated total reflectance-fourier transform infrared (ATR-FTIR) spectroscopy

ATR-FTIR spectroscopy serves as a valuable tool for acquiring insights into the chemical composition of binder samples, particularly as it undergoes specific chemical changes during the aging process. To prepare FTIR samples, approximately 1 g of the material was meticulously heated in a metal spoon above a heat gun until it reached a temperature of 110 °C. Subsequently, stirring was performed for 3 min using the tip of a thermometer. Small droplets of the material were then carefully transferred onto a silicon foil and covered with a lid to prevent contamination from dust or light-induced aging on the surface of the binder [24]. The measurements were conducted using a Nicolet iS5 Thermo Fisher Scientific instrument, equipped with an attenuated total reflection unit featuring a diamond crystal. Each spectrum was generated by collecting data from 24 scans, employing a resolution of 4 cm⁻¹. For each aging state, four samples were prepared and analysed in the solid state, resulting in four spectra per aging state in the range of 4000–400 cm⁻¹.

For extracted binder from mixture samples of the last two rows of Table 2, the measurements were conducted using a Frontier Perkin Elmer instrument. Each spectrum was generated by collecting data from 8 scans, employing a resolution of 4 cm⁻¹. For each aging state, one sample was prepared and analysed in the solid state, resulting in four spectra per aging state in the range of 650 – 4000 cm⁻¹.

The use of two different FTIR devices was due to the collaborative nature of this work between two institutes, which provided access to different instruments. Data from both devices were used to ensure a comprehensive analysis, with reproducibility confirmed through multiple measurements on the same samples. Sample preparation and measurement protocols were standardized to minimize discrepancies, ensuring consistent results.

The spectral data underwent pre-processing steps. Initially, an 8-point baseline correction was applied to address spectral shifts (Table 3S) [48]. Subsequently, a normalization step known as normalization to change the maximum to 1 (NMO) was conducted [49]. This step aims to standardize absorbance values across data collected from different devices by scaling them to a fixed range of 0 to 1. Specifically, the minimum point within the range of 2800–3200 is set to zero, and the maximum point is adjusted to 1 (Table 3S).

Table 3 lists the wavenumber ranges of main functional groups identified by the FTIR spectra. Equation (1) was used to calculate the indices for each functional group with the full area under the curve and the vertical limits mentioned in Table 3.

The computation of indices followed this equation:

$$\text{index} = A_x/A_{\text{Total}} \quad (1)$$

The symbol A_x denotes the peak area under the curve within specific

Table 2
Aging conditions for binder and mixture samples.

Sample	Variable	Thickness(mm)	Temperature (°C)	Pressure (bar)	Time (hour)	Humidity	# of samples
Q and T Binder	Temperature	1, 2, 3.2	60, 70, 85	20	20	<10 %, >99 %	18
Q and T Binder	Pressure	1, 2, 3.2 1 mm	85	1.5, 10,20 150	20	<10 %, >99 % <10 %	18 + 1
Q and T Binder	Duration	1, 2, 3.2 1	85	20	5,10,20 40,80	<10 %, >99 % >99 %	18 + 2
PA and SMA Mixture	Temperature	/	60, 85	20	20	<10 %, >99 %	8
PA and SMA Mixture	Pressure	/	85	150	20	<10 %	2

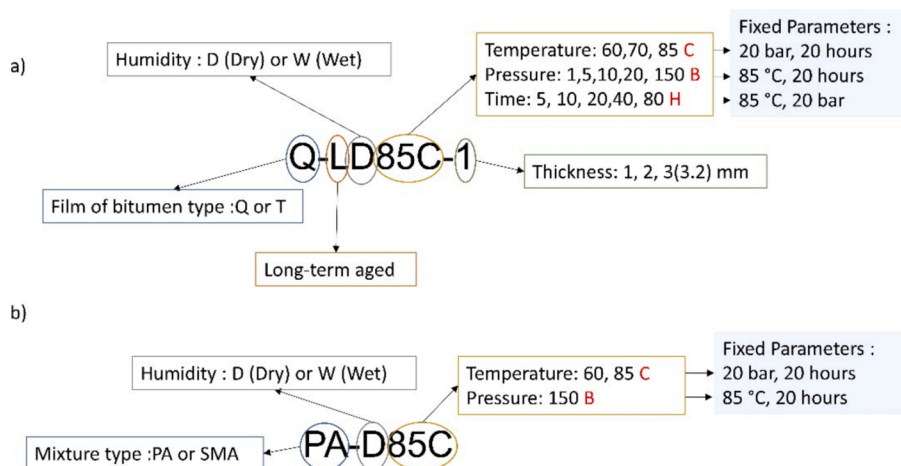


Fig. 1. Annotation used for a) binder samples and b) mixture samples, i.e. SMA and PA.

Table 3
Main functional groups of binder in FTIR spectra [50].

Area	Vertical band limit(cm^{-1})	Functional groups
A ₈₁₀	710–734 734–783 783–833 833–912	Hydrocarbon chain, $(\text{CH}_2)_n$, C–H in isolated/two/four adjacent hydrogen aromatic rings or C–CH ₂ rocking in alkyl side chains with more than four carbons
A ₁₀₃₀	984–1047	Oxygenated function-sulfoxide, S = O
A ₁₂₀₀	1100–1180 1280–1330	Tertiary alcohol C–C–O, C–O in carboxylic acid, C–C–C in diaryl ketones, C–N secondary amides, O = S = O in sulfone
A ₁₃₇₆	1350–1395	Branched aliphatic structures, CH ₃
A ₁₄₆₀	1395–1525	Aliphatic structures, CH ₃ and CH ₂
A ₁₆₀₀	1535–1670	Aromatic structure, C = C
A ₁₇₀₀	1660–1750	Oxygenated function-carbonyl, C = O
A ₂₉₅₃	2820–2880 2880–2990	Aliphatic structures, Symmetric, Asymmetric stretching, CH
A ₃₄₀₀	3100–3600	Hydroxyl stretching, OH, NH
A _{Total} = A ₈₁₀ + A ₁₀₃₀ + A ₁₂₀₀ + A ₁₃₇₆ + A ₁₄₆₀ + A ₁₆₀₀ + A ₁₇₀₀ + A ₂₉₅₃ + A ₃₄₀₀		

ranges outlined in Table 3.

3.2.2. Dynamic shear rheometer (DSR) – Frequency sweep

The Complex shear modulus (G^*) and phase angle (δ) were measured over a range of temperatures and frequencies using dynamic shear rheometer (DSR) with oscillatory loading. The DSR tests were completed with an 8-mm-diameter parallel plate and a 2-mm gap at temperatures range of 0 to 40 °C (with an increment of 10 °C). The tests were done in a frequency range from 15.9 to 0.0159 Hz (100 to 0.1 rad/s) and a strain load of 0.05 % and 0.1 % for 0–20 °C and 30–40 °C, respectively. These strain levels were selected based on the need to maintain measurements within the linear viscoelastic range of the binder while ensuring reliable data across the test temperature range. Lower temperatures (0–20 °C) typically yield higher binder stiffness, requiring a smaller strain load (0.05 %) to avoid exceeding the linear viscoelastic limit and risking non-linear responses that would compromise the accuracy of complex modulus (G^*) and phase angle (δ) measurements. At higher temperatures (30–40 °C), the binder becomes less stiff, allowing for a slight increase in strain (0.1 %) without surpassing the linear viscoelastic threshold. This approach aligns with the standard protocol (14770 2012) [51]), which supports strain adjustments according to the material's stiffness properties at various temperatures to maintain data integrity. Each sample was tested with two replicates to confirm repeatability and reliability of the results.

Based on the time–temperature superposition principle (TTSP),

master curves of complex modulus and phase angle were constructed at a reference temperature of 20 °C. Shift factors, typically denoted by “ a_T ”, are used in time–temperature superposition (TTS) to horizontally shift the binder response data obtained at various temperatures along the logarithmic frequency axis. The principle behind TTS is that the effects of temperature and frequency on the material's viscoelastic properties are equivalent. Therefore, multiple isothermal curves at different temperatures can be shifted into a single master curve at different frequencies, characterizing the material's behaviour across various conditions. The magnitude of the shift factors indicates the sensitivity of the binder's viscoelastic properties to temperature changes, with larger shift factors reflecting a greater temperature dependence.

The Sigmoidal Model, commonly employed to describe the rate dependency of the modulus master curve, has been extensively utilized by researchers to characterize the complex modulus master curve of asphalt mixtures and bituminous binders [52]. The model is mathematically represented as follows:

$$\log|G^*| = \sigma + \frac{\alpha}{1 + e^{\beta + \gamma(\log(\omega))}} \quad (2)$$

In this model, $\log(\omega)$ represents the log of the reduced frequency, σ (sigma) denotes the lower asymptote, and α (alpha) represents the difference between the upper and lower asymptotes. Parameters β (beta) and γ (gamma) define the shape of the curve between the asymptotes and the location of the inflection point, which is determined by $10^{(\beta/\gamma)}$ [53].

The α (alpha) parameter reflects the overall stiffness or viscoelastic properties of the binder. A higher alpha value suggests a stiffer binder, while a lower value indicates a more flexible binder. The beta parameter represents factors such as the temperature dependence of the binder's stiffness or the transition between different rheological regimes (e.g., from elastic to viscous behaviour). The gamma parameter denotes the sensitivity of the binder's stiffness to changes in frequency, with a higher gamma value indicating a more pronounced change in stiffness with frequency or strain rate. The sigma parameter represents the baseline stiffness of the binder or any inherent structural characteristics that influence its rheological behaviour.

In this study, the parameters of the sigmoidal model, the shift factors from the TTSP construction of master curves, and the crossover values (crossover frequency (CR-Fr) and crossover complex modulus (CR-CM)) were utilized for subsequent multivariate analysis. CR-Fr represents the frequency and CR-CM represents the complex modulus at which the phase angle is 45° and the storage modulus equals the loss modulus. These values provide insights into the viscoelastic transition of binder from fluid-like to solid-like behaviour.

3.3. Multivariate analysis

3.3.1. Principle component analysis (PCA)

PCA is a statistical technique used to reduce the dimensionality of data by transforming it into a set of uncorrelated variables, called principal components, that capture the most variance in the data. For the chemical-rheological analysis, PCA was employed to categorize samples according to binder type and the effects of aging. This was achieved by utilizing both chemical and rheological parameters, allowing for an assessment of the significance of these parameters in characterizing binder types and aging effects which is essential for classification and regression purposes. The dataset used for PCA analysis were constituted by both FTIR results, encompassing all the indices listed in Table 3, where four peaks in the range of 710–912 cm^{-1} were considered as separate indices, and DSR results, which includes four sigmoidal model parameters (alpha, beta, gamma, sigma), four shift factors at 0, 10, 30, and 40 °C, and the CR-Fr and CR-CM. In total, 20 features were selected as the input for the analysis instead of the entire FTIR spectra or master curves to avoid the curse of dimensionality.

To perform PCA, the scores of target samples are computed using the equation $\mathbf{Y} = \mathbf{X} \times \mathbf{W}$, where \mathbf{X} represents the dataset comprising m samples (grouped into l categories) and n variables. \mathbf{W} denotes an $n \times p$ loading matrix, with p indicating the number of selected principal components, while \mathbf{Y} forms an $m \times p$ score matrix describing the projection of \mathbf{X} into a p -dimensional feature space. To derive \mathbf{W} , the eigenvectors and eigenvalues of the covariance matrix of the variables within a spectral dataset are calculated. Subsequently, the eigenvalues are arranged in descending order, and p eigenvectors with the largest eigenvalues are chosen to construct \mathbf{W} . Additionally, PCA loadings are analysed to identify significant regions for cluster formation [43].

3.3.2. Multiple linear regression (MLR)

Multiple linear regression is a statistical method that models the relationship between a dependent variable and two or more independent variables by fitting a linear equation to the observed data. To evaluate the relationship between the independent variables—temperature, pressure, and time—during the aging process of bituminous binders, a multiple linear regression (MLR) approach was utilized. Moreover, MLR model was used to determine the relative influence of each aging condition on the aging indices and to capture the combined effects of temperature, pressure, and time on aging. This analysis focuses on Q binder samples, as further comparison with field samples, which contain only Q binder, will be conducted. A dataset comprising 52 lab-aged samples was employed for this purpose. The data points were divided into two subsets: thermo-oxidative and hygrothermal. The analyses were performed separately for thermo-oxidative and hygrothermal data. Each sub-dataset was further divided into three additional datasets based on the sample thickness. For further analysis, only the dataset with a thickness of 1 mm was considered, as it is the only group with a sufficient number of data points, with at least 10 points available for modelling.

The multiple linear regression (MLR) analysis was conducted using a combined index from FTIR and DSR as the dependent variable. This combined index was calculated for each sample by summing all standardized FTIR indices (as shown in Table 4) and DSR parameters, which included eight sigmoidal parameters and crossover values. The

Table 4
Estimated coefficient for each factor of Equation (10) based on MLR model.

Hygrothermal aging		
	Coefficient	P value
Constant (α_0)	-4.899	0.000
Temperature (α_1)	0.017	0.017
Pressure (α_2)	0.026	0.006
Time (α_3)	0.036	0.001

combined aging index considered whether the FTIR and DSR indices increased (+1) or decreased (-1) with aging during the summation process.

Once the combined aging index was calculated, it was plotted against the aging variables to check for a linear relationship. However, the plot (Fig. 3S) indicated that the relationship was more exponential, so the natural logarithm of the combined index was used for the MLR modelling. The purpose of the MLR was to quantify how aging conditions affected the combined index and to assess the relative influence of each condition on binder properties.

Interaction terms—accounting for the combined effects of temperature, pressure, and time—were not included to avoid overcomplicating the model, especially since only 8 to 10 data points were available. Including these terms could risk overfitting, capturing noise rather than the actual relationship. This simplified approach also helped explore whether high values of one variable could offset low values of another. Additionally, the model can be applied to back-calculate aging conditions that would produce similar aging levels as those observed in field samples. The regression models used in this analysis are shown in Equation (3).

$$\ln(\text{CombinedIndex}) = \alpha_0 + \alpha_1(\text{Temperature}) + \alpha_2(\text{Pressure}) + \alpha_3(\text{Time}) + \epsilon \quad (3)$$

where α_i are coefficients to be determined, and ϵ is the error term.

Prior to performing the MLR analysis, the Pearson correlation coefficient (Equation (4)) and Variance Inflation Factor (VIF) (Equation (5)) were calculated to evaluate the multicollinearity among the independent variables.

$$\rho_{xy} = \frac{\text{Cov}(x,y)}{\sigma_x \sigma_y} \quad (4)$$

ρ_{xy} is Pearson product-moment correlation coefficient, $\text{Cov}(x,y)$ is covariance between variables x and y , σ_x and σ_y are standard deviation of x and y , respectively.

$$\text{VIF}_i = \frac{1}{1 - R_i^2} \quad (5)$$

R_i^2 is unadjusted coefficient of determination for regressing the i th independent variable on the remaining ones. The correlation coefficient, a statistical measure of the strength of a linear relationship between two variables, ranges from -1 to 1. A correlation coefficient of -1 signifies a perfect negative or inverse correlation, indicating that values in one series rise as those in the other decline, and vice versa. Variance inflation factors provide a rapid assessment of the extent to which a variable contributes to the standard error in regression analysis. A VIF exceeding 10 indicates the presence of substantial multicollinearity, necessitating alternative measures to address this issue. In cases of significant multicollinearity, the variance inflation factor will be notably high for the involved variables. This preliminary analysis was essential to verify the independence of the predictors.

3.3.3. Pairwise Euclidean distance

Pairwise Euclidean distance is a metric that quantifies the straight-line distance between each pair of points in a dataset within a Euclidean space. To identify the laboratory conditions that are closest to the field samples, pairwise distances were calculated based on the first three principal components [54]. Euclidean distance was used to measure the straight-line pairwise distance between two points in the selected three-dimensional space, where the distance between two points (p_1, p_2, \dots, p_d) and (q_1, q_2, \dots, q_d) is computed as follows in Equation (6):

$$\text{Euclidean distance} = \sqrt{(p_1 - q_1)^2 + (p_2 - q_2)^2 + \dots + (p_d - q_d)^2} \quad (6)$$

3.3.4. Support vector regression (SVR)

Support vector regression (SVR) is a machine learning method that aims to find a hyperplane in a high-dimensional space that best fits the target values within a specified margin width, ϵ , allowing deviations from actual values to be no larger than ϵ . Slack variables, ξ_i and ξ_i^* , are introduced to account for deviations beyond this margin [47]. The SVR method was chosen to leverage its capability in handling non-linear relationships and providing robust predictive performance for the specified tasks. SVR was utilized in two distinct applications: predicting rheological parameters based on FTIR indices and training a model to estimate the duration of field aging a laboratory sample simulates. The former included FTIR indices as input dataset while the latter used laboratory sample data for field aging estimation. SVR seeks to minimize both the coefficients of the hyperplane (to ensure flatness) and the sum of the slack variables (to reduce errors) simultaneously (Equations (7) and (8)):

$$\text{minimize } \frac{1}{2} \|w\|^2 + C \sum_{i=1}^l (\xi_i + \xi_i^*) \quad (7)$$

$$\text{Subject to } \begin{cases} y_i - w^T x_i - b \leq \epsilon + \xi_i \\ w^T x_i + b - y_i \leq \epsilon + \xi_i^* \\ \xi_i, \xi_i^* \geq 0 \end{cases} \quad (8)$$

In this context, w represents the feature vector, b is a constant, and x_i and y_i are the independent and dependent variables in \mathbf{X} and \mathbf{Y} , respectively. The constant $C > 0$ balances the trade-off between the flatness of the hyperplane and the deviations from the marginal range [55]. A high value of C emphasizes correct prediction of all training examples, which is not recommended for datasets with many noisy observations.

Kernel functions, such as linear, polynomial, radial basis function (RBF), can be used to preprocess \mathbf{X} , facilitating the effective description of non-linear relationships between predictors and responses. When employing kernel functions, the kernel coefficient γ (gamma) must be determined, as it defines the influence of a training sample on the regression process. A high γ value indicates better fitting of the training data but comes with the risk of overfitting.

The SVR model was initially optimized through hyperparameter tuning, a process of optimizing the set of hyperparameters (C , ϵ , kernel, gamma). This process was conducted using grid search, which involves specifying a set of possible values for each hyperparameter and systematically evaluating the model's performance for every combination of these values. The optimized hyperparameters, which provide the best performance on a validation set (a subset of data used during model training to tune parameters and prevent overfitting), improve the model's generalizability to unseen data (new data that the model has not encountered during training or validation, typically referring to the test set or real-world data).

3.3.5. Model validation

For the SVR analysis of predicting rheological parameters, the dataset of 60 data points was split into training (70 %) and testing (30 %) sets using the scikit-learn library in Python, with a fixed random state to ensure reproducibility. A 10-fold cross-validation strategy was applied, wherein the dataset was divided into 10 equal segments. Nine segments were used for model training, and one segment was reserved for testing, iterating this process 10 times with a different testing segment each iteration. The accuracy outcomes were averaged to provide a robust evaluation of the model's effectiveness.

The regression model's performance was evaluated using several metrics to ensure a comprehensive assessment. These metrics include the root mean square errors of calibration ($RMSEC$), cross-validation ($RMSECV$), and prediction ($RMSEP$) (Equation (9)), along with the determination coefficients of calibration (R_c^2), cross-validation (R_{cv}^2), and

prediction (R_p^2) (Equation (10)), and the relative percent difference (RPD) (Equation (11)) [47].

$$RMSE = \sqrt{\frac{1}{N} \sum_{i=1}^N (\hat{y}_i - y_i)^2} \quad (9)$$

$$R^2 = 1 - \frac{\sum_{i=1}^N (\hat{y}_i - y_i)^2}{\sum_{i=1}^N (y_i - \bar{y}_i)^2} \quad (10)$$

$$RPD = \frac{SD}{RMSE} \quad (11)$$

In these evaluations, y_i and \hat{y}_i represent the measured and predicted values for sample i , \bar{y}_i is the mean value of y_i , N denotes the number of samples for calibration, cross-validation, or prediction, SD is the standard deviation of measured values for N samples.

RPD indicates the model's predictive ability relative to data variability. An RPD value higher than 2 implies good model accuracy, while an RPD larger than 3 indicates excellent performance [56]. The Coefficient of Determination (R^2) quantifies the proportion of variance in the dependent variable predictable from the independent variables, $RMSE$ measures the average magnitude of prediction errors, and RPD is the ratio of the standard deviation of the training data to the $RMSE$, indicating model predictability. These metrics were used in parallel to provide different perspectives on the model's performance, allowing for a thorough evaluation and comparison of all models to identify the most robust and accurate one for our specific objectives.

When applying SVR to the prediction of equivalent field ageing time of a laboratory sample, Leave-One-Out Cross-Validation ($LOOCV$) was employed due to the limited field data (8–10 points). $LOOCV$ uses one observation as the validation set and the remaining observations as the training set, repeating this process for each observation in the dataset. The $RMSE$ was calculated and reported to evaluate the model performance.

For the MLR analysis of aging factors, the $LOOCV$ was also used considering the limited number of field samples involved.

Fig. 2 shows the methodology flowchart used in this work. The details of each section are extensively explained in the material and method section.

4. Results and discussion

4.1. Attenuated total reflectance-fourier transform infrared (ATR-FTIR) spectroscopy

FTIR spectra of some of the lab-aged and field-aged samples, before and after preprocessing, are plotted in Fig. 3. As observed, the main changes in the spectra of samples with varying aging conditions occur in the range of carbonyl and sulfoxide region, consistent with the finding from literature that sulfoxide and carbonyl indices are the most informative indices for oxidative aging effects [57]. Therefore, for the evaluation of the effects of various factors including pressure, time, and thickness on aging, sulfoxide and carbonyl indices will be utilized. Fig. 4S – 6S in supporting information show the mean values of the carbonyl and sulfoxide indices.

4.1.1. Effect of aging factors on chemical properties of binders

4.1.1.1. Temperature factor. Fig. 4S shows sulfoxide and carbonyl indices of binder samples at different aging temperatures. Higher temperature led to higher sulfoxide and carbonyl indices in the binder. Hygrothermal aging resulted in higher indices than thermo-oxidative aging, especially at higher temperatures and thinner films. The indices increased with decreasing binder film thickness for both Q and T binders, especially at 85 °C. Notably, hygrothermal aged samples at

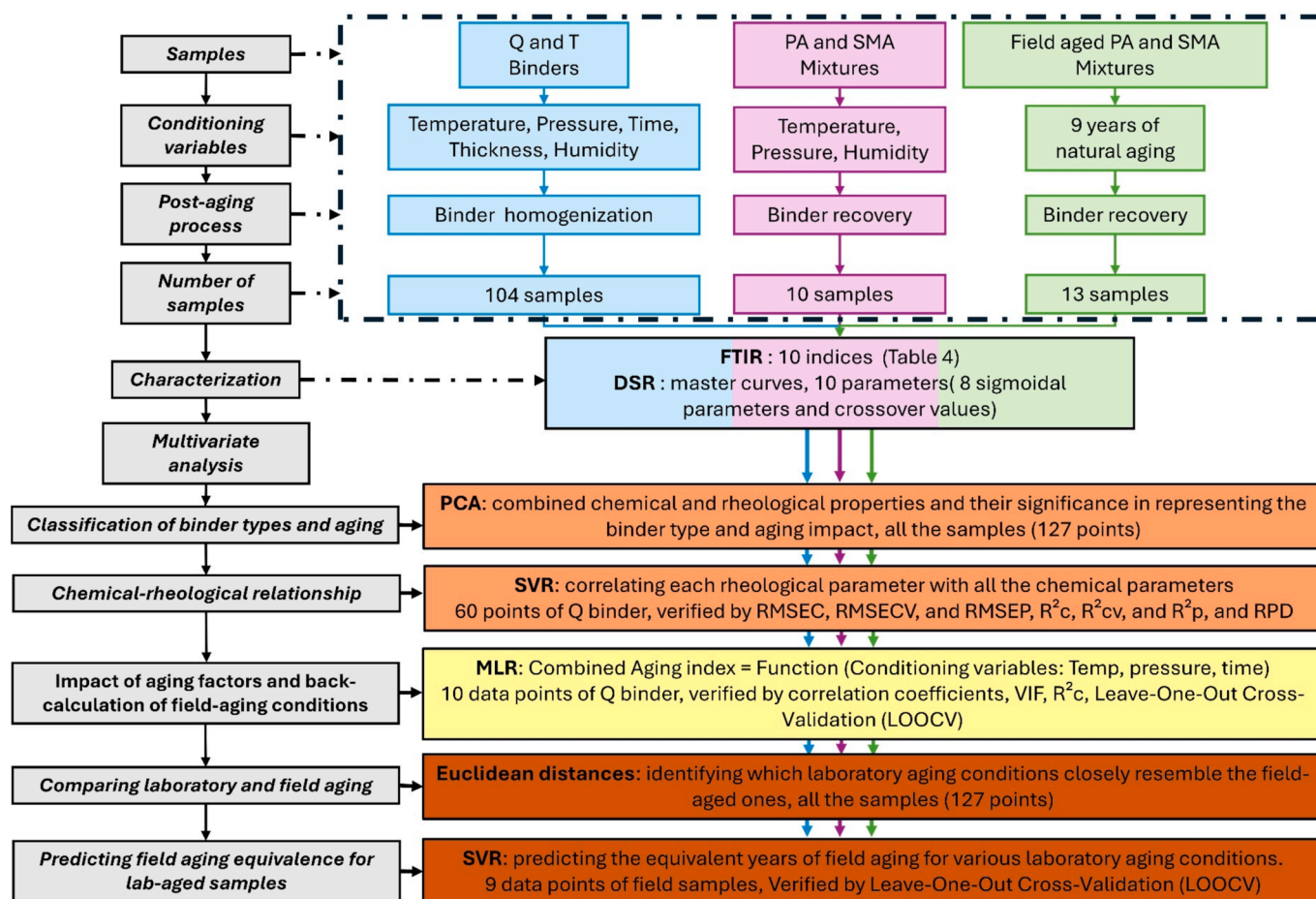


Fig. 2. Methodology flowchart including sample preparation, aging conditions variables, post aging process, number of obtained samples, characterization with FTIR and DSR, and Multivariate analysis steps.

85 °C exhibited a sharp rise in the carbonyl index, particularly in 1 mm thick samples, indicating that high temperature and hygrothermal aging of thin films represent the most severe aging condition.

Fig. 4 presents the combined FTIR index as a function of aging temperature. The FTIR index changes exponentially with temperature under both hygrothermal and thermo-oxidative aging conditions, consistent with previous studies [5]. Furthermore, compared to thermo-oxidative aging, the Q binder exhibits a higher power under hygrothermal aging, indicating an accelerating effect of humidity on aging at higher temperatures. In contrast, the T binder did not display an accelerating effect of humidity on aging at higher temperatures.

4.1.1.2. Pressure factor. Carbonyl and sulfoxide indices of Q and T samples at different pressures (1, 5, 10, 20, and 150 bar) are shown in Fig. 5S. The carbonyl and sulfoxide indices increased with rising pressure, indicating more severe aging for higher pressure. Higher indices are observed for hydrothermally aged samples compared to thermo-oxidative aged samples at higher pressure, with a more noticeable increase in both indices is shown for samples with 1 mm thickness. This suggests that the presence of water vapor, combined with harsh aging conditions such as higher pressure or thinner films, accelerates binder oxidation more effectively than thermo-oxidative aging alone. The difference between hygrothermal and thermo-oxidative aging was more pronounced in Q samples than in T samples.

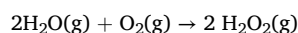
Fig. 5 depicts the combined index at various pressures for samples with 1 mm thickness. A logarithmic correlation between the index and pressure was revealed, indicating that aging increases with pressure, but at a decreasing rate. This suggests a threshold beyond which higher

pressure has limited impact on binder oxidation. Additionally, different sensitivities of Q and T binders to pressure with and without humidity were observed. The higher coefficient for hygrothermal aging compared to thermo-oxidative aging in the Q binder indicates that pressure has a more substantial effect on aging in the presence of humidity, while for T binder, humidity caused limited changes.

4.1.1.3. Time factor. Besides temperature and pressure, aging time was evaluated at 5, 10, and 20 h (Fig. 6S a-d). Sulfoxide and carbonyl indices increased with aging time for all Q and T samples (Fig. 6S). Hygrothermal aging resulted in a higher carbonyl index after 20 h compared to thermo-oxidative aging, indicating its greater effectiveness within this time frame. Thin films exhibited higher indices than thick films, suggesting that thicker films require more time to reach similar index values. For durations of 40 and 80 h, the indices continued to rise, indicating the formation of more aging products with longer exposure times.

As show in Fig. 6, the combination of carbonyl and sulfoxide indices showed faster hygrothermal aging during the initial 20 h at 85 °C compared to thermo-oxidative aging.

This suggests that humidity accelerates the reaction, possibly due to hydrogen peroxide formation:



The potential formation and infiltration of H_2O_2 molecules into the binder binders can accelerate the oxidation of polycyclic perhydroaromatics [5]. However, the activation energy for this reaction is typically high, and further studies are needed to confirm the effectiveness of the

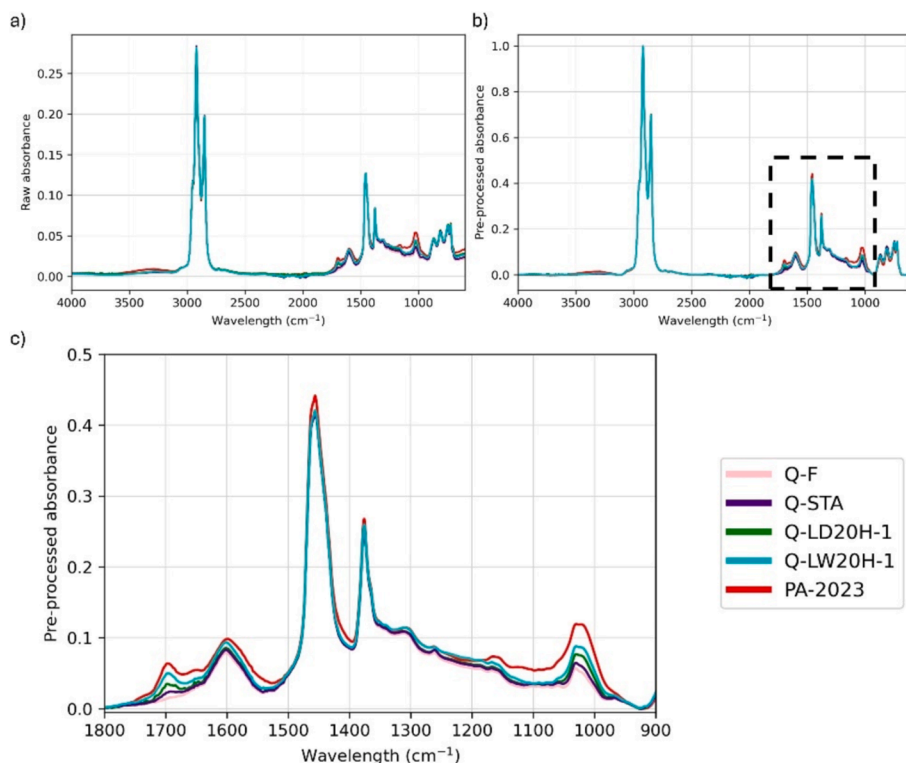


Fig. 3. FTIR spectra illustrating fresh, short-term aged, long-term aged (with and without humidity), and a 9-year field-aged sample are presented in: a) raw spectral form, b) baseline-corrected and normalized spectra, and c) the 900–1800 cm^{-1} region to highlight variations in carbonyl and sulfoxide peaks.

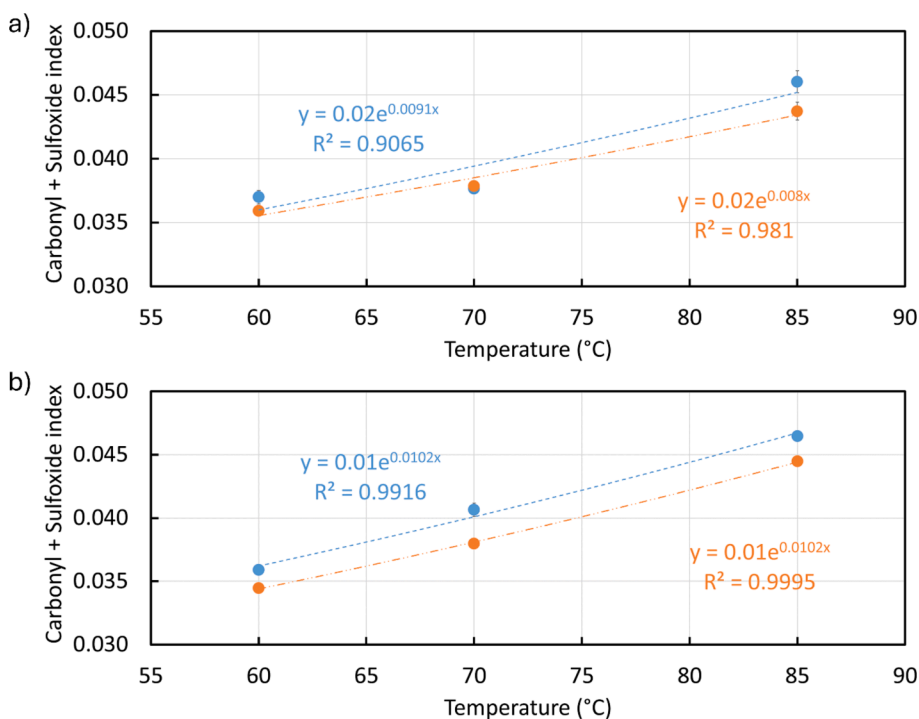


Fig. 4. Summation of carbonyl and sulfoxide indices versus aging temperature for a) Q and b) T binders with a thickness of 1 mm. Blue color represents the hydrothermally aged samples and orange color represents the thermo-oxidatively aged samples. (For interpretation of the references to color in this figure legend, the reader is referred to the web version of this article.)

aging conditions for producing significant amounts of hydrogen peroxide without a catalyst in the dark.

Before 20 h, a linear relationship between FTIR indices and time is

observed. For durations beyond 20 h, a linear relationship with a smaller slope was observed (Fig. 6), consistent with prior studies [58,59]. The two different slopes suggest two phases in long-term hydrothermal

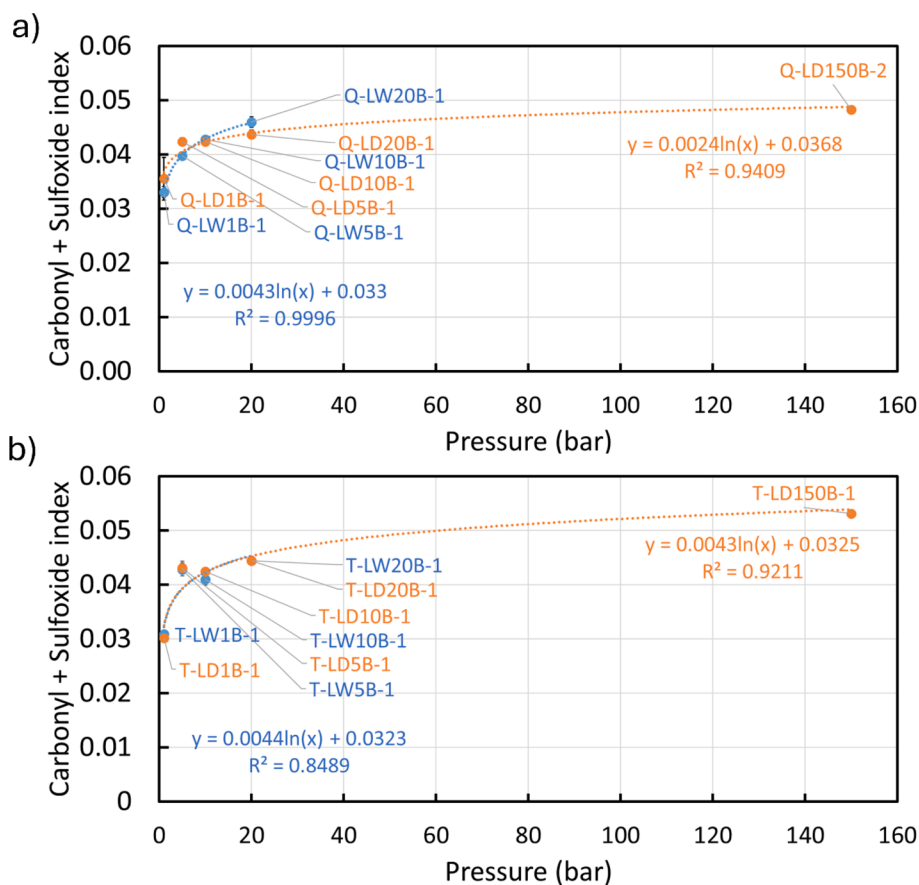


Fig. 5. Summation of carbonyl and sulfoxide indices versus pressure for a) Q binder and b) T binder. The data for hydrothermal aging and thermo-oxidative aging is shown in blue and orange, respectively. (For interpretation of the references to color in this figure legend, the reader is referred to the web version of this article.)

aging: an initial fast phase followed by a slower phase. Aging time less than 20 h reveals faster reaction due to higher availability of oxidizable molecules at the onset of the reaction.

4.1.2. Effect of aging factors on chemical properties of recovered binders of laboratory aged mixtures

4.1.2.1. Temperature factor. Fig. 7 shows the carbonyl and sulfoxide indices of mixture samples aged at 60 °C and 85 °C. Increasing the temperature increased both indices for both types of mixtures. For porous asphalt (PA), adding humidity during aging significantly increased both indices. In contrast, stone mastic asphalt (SMA) aged at 60 °C shows no difference between hydrothermal and thermo-oxidative aging. At 85 °C, SMA aged with humidity shows less aging than in thermo-oxidative conditions. This can be attributed to the higher air voids in PA, which allow greater oxygen access and interaction of humidity-induced intermediates with the binder. SMA samples show less aging under hydrothermal conditions due to fewer voids, limiting oxidative molecule penetration and exposing only the sample surface to reactive components. Thus, hydrothermal aging accelerates aging more in PA compared to SMA.

4.1.2.2. Pressure factor. Mixture samples were aged under different pressures (20 and 150 bar) as shown in Fig. 8 a-b. By increasing pressure, the carbonyl index increased sharply, while the sulfoxide index changed slightly, consistent with the results for binder samples after thermo-oxidative aging at these pressures. Comparing the sulfoxide indices of PA and SMA aged at 85 °C under 20 and 150 bar shows that SMA contains slightly more oxidative products. Despite the higher air voids of PA, the denser structure of SMA might retain heat more effectively,

accelerating oxidative aging at higher pressures. These preliminary results suggest further experiments with additional repetitions and CT scans to examine air void connectivity and oxygen distribution are necessary for comprehensive analysis.

4.1.3. Effect of field aging on chemical properties of mixture samples

The chemical composition of PA and SMA samples during 9 years of field aging were investigated using FTIR and the results are shown in Fig. 7. For PA samples, both carbonyl and sulfoxide indices increased with time (Fig. 9). Notably, the carbonyl index after 4 years of aging is unexpectedly higher than that of 5 to 9 years, likely due to the complexity of field aging. For SMA, samples from years 5 to 9 show minimal differences in indices. The sum of both indices exhibits a linear relationship with time for both PA and SMA (Fig. 7S). This field data will be compared with lab-aged samples in subsequent sections.

4.2. Dynamic shear rheometer (DSR) – Frequency sweep

4.2.1. Effect of aging factors on rheological properties of binders

4.2.1.1. Temperature factor. The frequency sweep test was conducted for all binder samples and their master curves are presented in Fig. 8S-10S. Fig. 8S shows the effect of temperature, with a higher temperature increasing G^* and decreasing phase angle. Moreover, Fig. 9S and 10S illustrate the impact of hydrothermal and thermo-oxidative aging on Q and T binders, respectively. At 60 °C and 85 °C, Q samples aged with humidity exhibited higher G^* and lower phase angle for each thickness. As expected, the 1 mm films showed more severe aging than the 2 mm and 3.2 mm films. Interestingly, Q samples aged at 70 °C showed overlapping results for hydrothermal and thermo-oxidative aging across

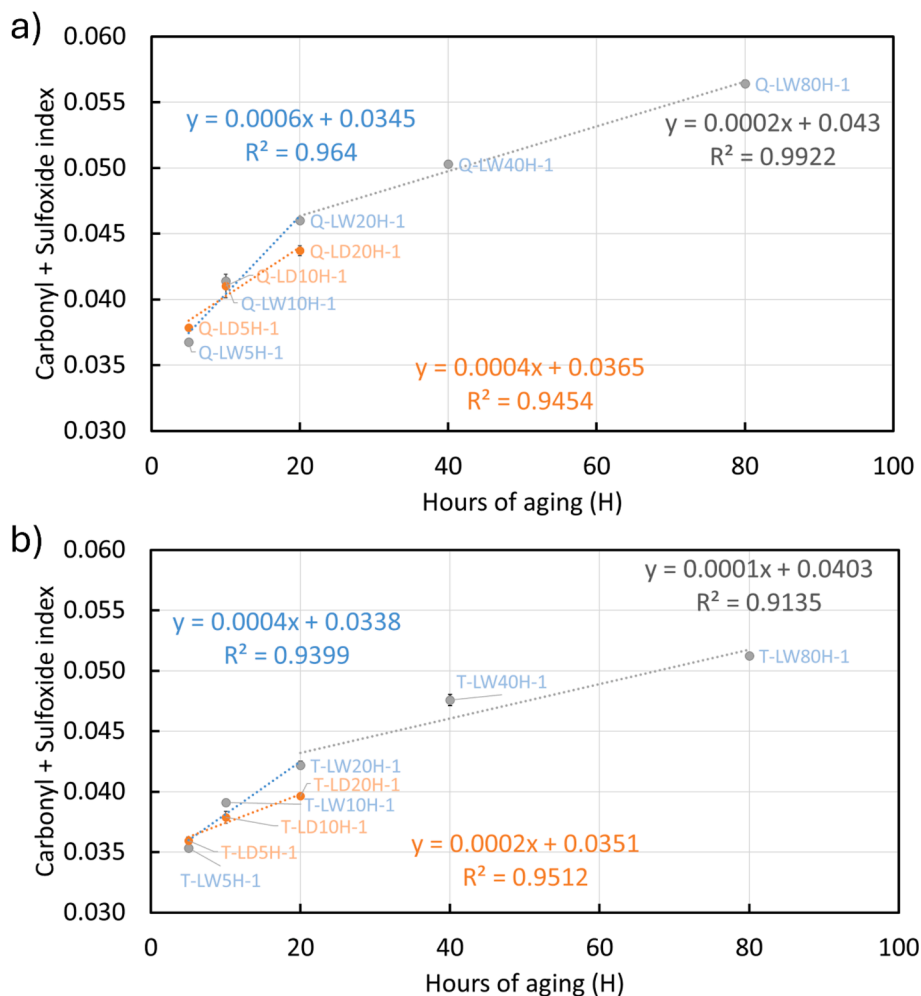


Fig. 6. Summation of carbonyl and sulfoxide indices versus aging time (Hours) for a) Q binder, b) T binder. Blue and orange colors represent the hydrothermal aged and the thermo-oxidative aged samples, respectively. (For interpretation of the references to color in this figure legend, the reader is referred to the web version of this article.)

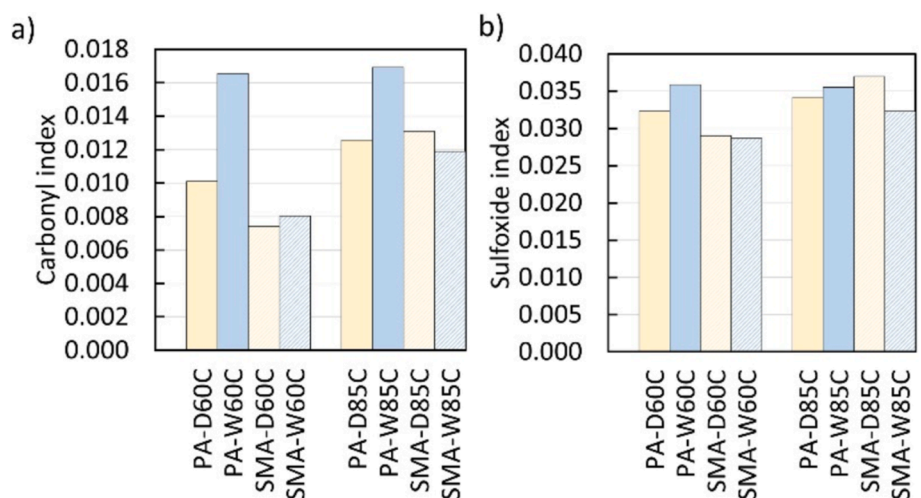


Fig. 7. FTIR results for mixture samples, a) carbonyl index, b) sulfoxide index. The samples were aged in a PAV under hydrothermal (W) and thermo-oxidative (D) conditions at 60 and 85°C for 20 h under 20 bar pressure.

all thicknesses. The effect of hydrothermal aging on Q binder is predominantly visible at low frequencies, suggesting greater resistance to deformation under slow-loading conditions like heavy, slow-moving

traffic, potentially improving performance against permanent deformation (rutting). Conversely, under fast-loading conditions like high-speed traffic and temperature fluctuations, the convergence at high

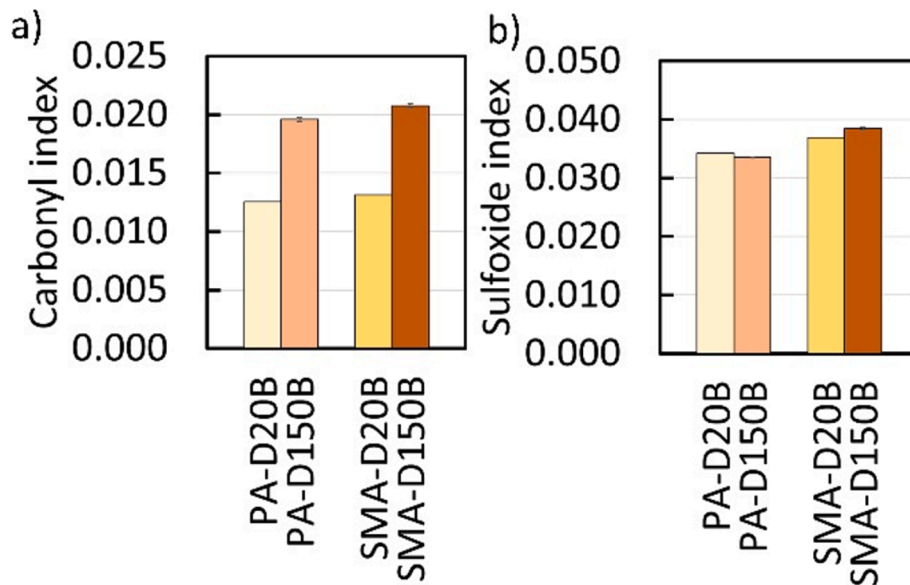


Fig. 8. FTIR results, for the effect of different pressures of 20 and 150 bar. The results are presented for PA and SMA mixture samples after thermo-oxidative (D) aging at 85 °C for 20 h, a) carbonyl index, b) sulfoxide index.

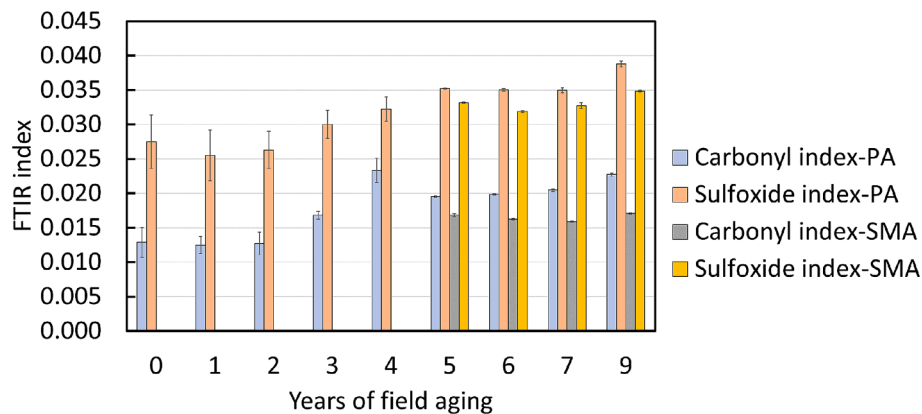


Fig. 9. FTIR results, effect of field aging on PA and SMA mixture samples. In 2022 (year 8) no sampling was performed and for SMA samples, those from 2019 (year 5) to 2023 (year 9) were available.

frequencies implies comparable resistance to cracking for both hygrothermal and thermo-oxidative aged samples. The most severe aging condition for Q binder was observed in the 1 mm film aged with humidity at 85 °C and 20 bar. For T binder, the results showed slight differences. At 60 °C, samples displayed more aging at low frequencies for thinner films with humidity. T samples aged at 70 °C and 85 °C demonstrated similar outcomes for hygrothermal and thermo-oxidative aging. The impact of different film thicknesses was evident, with the 1 mm films exhibiting the most aging. The most severe aging condition was observed in samples aged at 85 °C. The DSR results are consistent with the FTIR findings for both Q and T binders.

Moreover, two key parameters were calculated: crossover frequency (CR-Fr) and crossover complex modulus (CR-CM). Crossover values are significant points on the viscoelastic spectrum, independent of test frequency and temperature. Previous research indicates that lower CR-Fr values in aged binder correlate with higher molecular mass, longer relaxation time, and higher softening point [14,60]. Lower CR-CM values suggest higher polydispersity due to a wider distribution of molecular masses. Higher crossover frequency indicates more elastic behaviour at higher frequencies, contributing to better resistance against permanent deformation or rutting, especially under repetitive traffic loading. Higher crossover modulus indicates greater stiffness at

the crossover frequency, also enhancing resistance to rutting.

Fig. 10 a-b presents the CR-CM versus CR-Fr for samples at different temperatures, revealing Q-LW85C-1 and T-LD85C-1 as having the lowest CR-Fr and CR-CM values, indicating their most severe aging. This underscores the varying sensitivity to hygrothermal aging for different binders. Elevated aging at 85 °C was identified as a major factor in the aging of thin films, particularly those with a thickness of 1 mm. Additionally, incorporating humidity during aging was shown to be beneficial for binders sensitive to hygrothermal conditions. A linear relationship was found between crossover values, regardless of binder type or aging conditions.

4.2.1.2. *Pressure factor.* The effect of varying pressures (1, 5, 10, 20, and 150 bar) for both Q and T binder on different binder thicknesses is presented in Fig. 11S – 13S. As pressure increases, the gap between long-term and short-term aged samples widens, showing a marked increase in G^* and a decrease in phase angle, highlighting the severe impact of elevated pressure on binder aging. The effect of hygrothermal aging at higher pressures is observable in the phase angle master curves at lower frequencies for Q binder, aligning with previous observations on temperature effects showing lower sensitivity of T binder to hygrothermal aging. 1 mm films experience the most significant aging, with

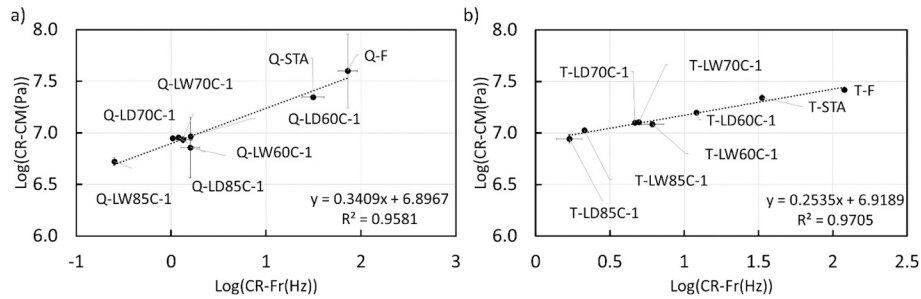


Fig. 10. Crossover complex modulus versus crossover frequency of 1 mm samples aged at different temperatures, i.e., 60, 70, 85 °C after hydrothermal (W) and thermo-oxidative (D) aging, a) for Q binder and b) for T binder.

higher G^* values and lower phase angle values. Interestingly, samples aged at 150 bar do not show significant changes in G^* or δ values, suggesting that extremely high pressure does not necessarily cause harsher aging in binders. This rheological observation aligns with FTIR results, indicating that a limited number of reactive sites in the binder might render extremely high pressure unnecessary for accelerated aging protocols. For the Q binder, the distances between master curves are larger compared to the T binder, indicating higher pressure sensitivity.

Crossover values in Fig. 11 a–b illustrate the linear relationship between these values for both binders. The Q binder shows overlapping crossover values for aged samples, while the T binder exhibits clear differences between aged samples at different pressures. The Q binder displays similar results for samples aged at 20 and 10 bar under hydrothermal conditions, whereas the T binder shows more aging for samples aged at 20 bar. Notably, the Q binder film aged at 20 bar under thermo-oxidative conditions shows significant error bars, indicating substantial variation between repetitions. Future research should investigate the reasons for this variability.

4.2.1.3. Time factor. The influence of aging time on the rheological properties of both Q and T binders was presented (Fig. 14S – 16S). Aging durations of 5, 10, and 20 h were chosen for both hydrothermal and thermo-oxidative conditions, with extended durations of 40 and 80 h for hydrothermal aging. By increasing aging time, the G^* increases while the phase angle decreases, indicating a greater aging impact. For the Q binder, the differences between hydrothermal and thermo-oxidative aged samples became more pronounced with longer aging. In contrast, the T binder showed no significant effect from humidity, regardless of aging duration, indicating higher sensitivity of Q binder to hydrothermal aging. The results show that 1 mm films exhibit the most aging, with increased G^* values and decreased phase angle values. Aging effects were more pronounced at low frequencies.

Crossover values plotted in Fig. 12 a–b show that longer durations reduce both CR-CM and CR-Fr, indicating more aging in binder films, with a linear relationship between these values. Similar to the master curves, crossover values indicate that T binder is less sensitive to hydrothermal aging, while Q binder shows greater sensitivity to the

presence of humidity during aging.

The DSR investigations indicate that the severity of hydrothermal aging depends on the binder's sensitivity to humidity during aging. Thinner films aged at high temperatures for longer durations show greater increases in G^* and more significant reductions in phase angle and crossover values. For pressure, samples aged at 20 bar exhibit similar results to those aged at 150 bar, suggesting that 20 bar is sufficient for future binder aging studies, and higher pressures are unnecessary to accelerate aging. Furthermore, crossover values and lower frequencies are more effective in distinguishing differences between aged samples than higher frequencies and the entire master curve. Thus, using lower frequencies and crossover values is recommended for comparing aging conditions in future studies.

4.2.2. Effect of aging factors on rheological properties of asphalt mixtures

Comparing the master curves of G^* and phase angle for PA and SMA mixtures aged at 60 °C and 85 °C in a PAV under hydrothermal and thermo-oxidative conditions shows that by increasing temperature, G^* increases and phase angle decreases (Fig. 17S). For PA samples at 60 °C, no significant differences are observed between hydrothermal and thermo-oxidative aging, while at 85 °C, hydrothermal aging results in lower phase angles and higher G^* values. SMA samples show overlapping master curves with fresh and short-term aged samples, likely due to the softening effect of extraction solvents [61]. PA samples exhibit lower phase angles and higher G^* values than SMA, indicating more aging, particularly at 85 °C. phase angle is more sensitive to aging, especially at intermediate frequencies. The effect of pressure on mixture samples during thermo-oxidative aging indicates that increasing pressure from 20 to 150 bar decreases phase angle and increases complex modulus, showing harsher aging (Fig. 18S). PA samples show more aging than SMA due to higher air voids, with differences diminishing at 150 bar due to the forcing of oxygen into samples. Medium pressures like 20 bar are recommended for mimicking field aging over extreme pressures like 150 bar.

Fig. 13 shows crossover values of lab-aged mixture samples, which differentiate samples more clearly than master curves. Thermo-oxidative conditioning ages SMA samples more than hydrothermal

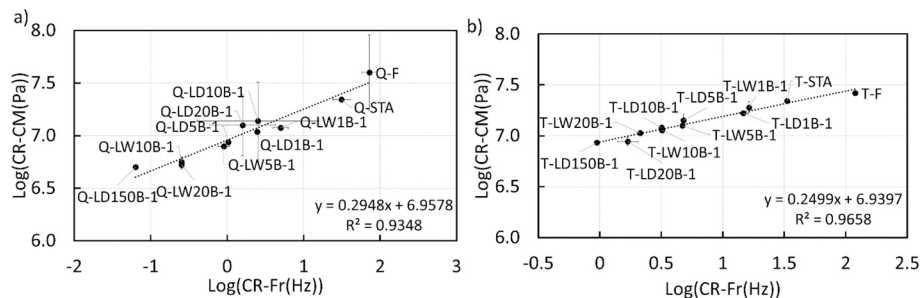


Fig. 11. Crossover complex modulus versus crossover frequency of 1 mm samples aged at different pressures, i.e., 1, 5, 10, 20, 150 bar after hydrothermal (W) and thermo-oxidative (D) aging, a) for Q binder and b) for T binder. Aging at 150 bar was performed only with thermo-oxidative aging.

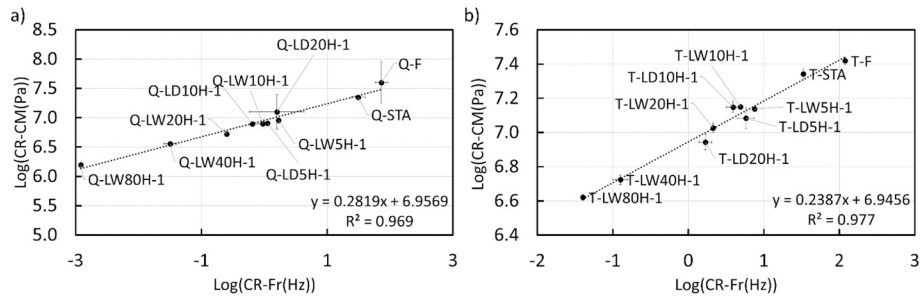


Fig. 12. Crossover complex modulus versus crossover frequency of 1 mm samples aged at different aging durations, i.e., 5, 10, 20, 40, 80 h after hydrothermal (W) and thermo-oxidative (D) aging, a) for Q binder and b) for T binder. Aging for 40 and 80 h was performed only under hydrothermal aging.

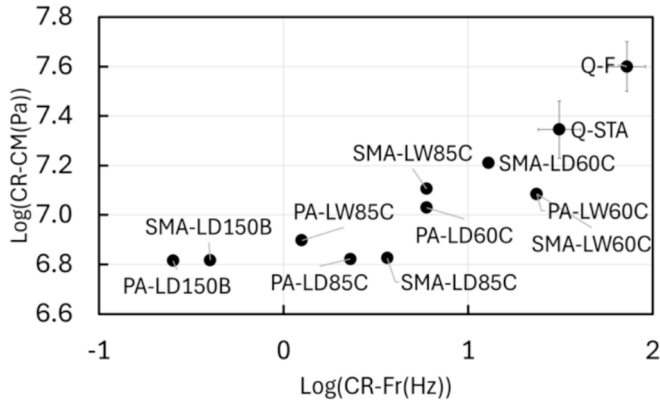


Fig. 13. Crossover complex modulus versus crossover frequency of PA and SMA asphalt mixture samples hydrothermally (W) and thermo-oxidatively (D) aged at different temperatures, i.e., 60 and 85°C and thermo-oxidative (D) aging under elevated pressure of 150 bar.

aging, independent of temperature, due to fewer air voids in SMA samples and reduced oxygen availability in the presence of humidity. PA samples show more aging for hydrothermal conditions at 85 °C. Both temperature and pressure reduce crossover values, aligning with observations from master curves.

4.2.3. Effect of field aging on mixture samples

Investigating the master curves of field-aged porous asphalt over 0 to 8 years (Fig. 19S) reveals that the phase angle decreases and G^* increases over time. Notably, the most significant changes occur during the initial four years, with more gradual changes in the final four years. This indicates that the initial stage of long-term field aging is more rapid. For SMA samples, master curve values are similar from years 5 to 8, with only the 8-year sample showing a slight reduction in phase angle and an

increase in G^* . Similar conclusions can be drawn from the crossover values (Fig. 14), which align with the observation of hydrothermal aged samples, where a reduction in the slope of FTIR indices versus time was noted for longer aging durations.

4.3. Multivariate analysis

4.3.1. Chemical and rheological features importance for aging pattern recognition by PCA

The PCA analysis was performed on binder samples using their combined chemical and rheological properties as input. Based on the explained variance, the first two principal components account for more than 80 % of the variance in the data (Fig. 20S). Therefore, a two-dimensional plot of PC1 versus PC2 (Fig. 15) can effectively represent the input data. As shown in Fig. 15, there is a clear distinction between Q

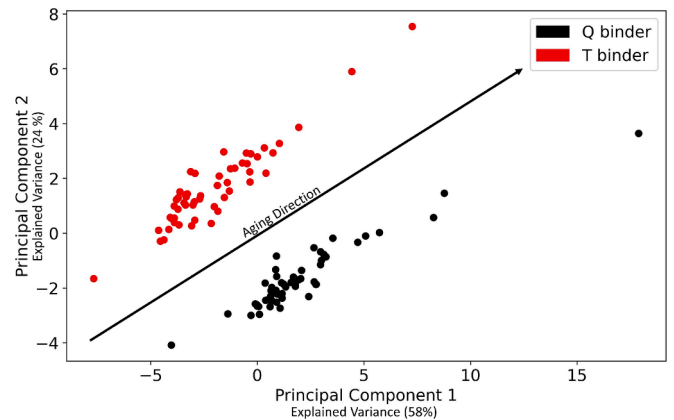


Fig. 15. PCA score plot of both Q and T binder types based on FTIR + DSR input data. The interactive plot can be found in Fig. 21S with annotated samples.

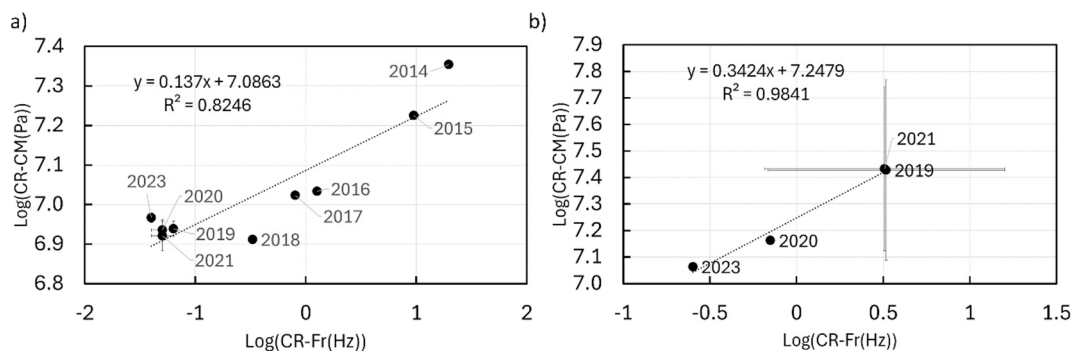


Fig. 14. Crossover complex modulus versus crossover frequency of field aged PA and SMA mixtures during 2014 to 2023, a) for PA mixture and b) for SMA mixture. In 2022 no sampling was performed and for SMA samples, those from 2019 to 2023 were available.

and T binder samples. Moreover, the aging direction trends towards the top right quadrant, indicating an increase in aging with both PCs.

PCA loadings are the coefficients that represent the contribution of the original variables to the principal components. A variable with a high absolute loading signifies its more significant influence on the principal component, and thus on the classification of binder type and aging state. In this study, loadings were normalized to a range of -1 to $+1$, and a threshold of ± 0.8 was set, with values beyond this threshold considered important. The sign of the loading—positive or negative—indicates whether the variable is positively or negatively correlated with the principal component.

Fig. 16 presents the loadings of all features for the first principal component (PC1). The importance of the PC1 axis lies in aging direction of both Q and T binders. Key contributors to PC1 include beta (transition between viscous and elastic regimes), gamma (sensitivity of the binder's stiffness to changes in frequency), the shift factor at 10 and 30 °C, crossover values (viscoelastic transition of binder from fluid-like to solid-like behaviour) from rheological measurements, along with FTIR indices in the range of 734–833 cm^{-1} (C–H bending vibrations in four or two adjacent hydrogen aromatic rings), 1100–1330 cm^{-1} (C–C–O in tertiary alcohol, C–O in carboxylic acid, C–C–C in diaryl ketones, C–N secondary amides, O = S = O in sulfone), and 2820–2990 cm^{-1} (C–H of methine, methylene, and methyl groups).

Fig. 17 presents the loadings of all features for PC2. The importance of the PC2 axis lies in both aging direction and differentiating between Q and T binders. Key contributors to PC2 include beta (transition between viscous and elastic regimes) and the shift factor at 10 °C from rheological measurements, along with FTIR indices in the ranges of 833–912 cm^{-1} (C–H in isolated adjacent hydrogen aromatic rings), 1535–1670 cm^{-1} (C = C in aromatics (ring mode)), 1660–1750 cm^{-1} (C = O in saturated carboxylic acids and C = O in saturated esters), and 2820–2990 cm^{-1} (C–H of methine, methylene, and methyl groups).

Both components highlight how aging impacts the viscoelastic properties and molecular structure of the binders, enabling effective differentiation between the two types. Key contributors include rheological measurements and FTIR spectral data, suggesting that changes in chemical structure correlate with aging and binder performance. This understanding could facilitate the development of predictive models that integrate these parameters, enhancing material selection and formulation strategies for specific applications.

To further understand the correlation between different aging

conditions, Q binders and Q mixture samples (PA and SMA) aged in both laboratory and field were used for PCA. It is shown that over 80 % of the variance in the input data can be explained by the first two principal components (Fig. 22S). Fig. 18 depicts the PC1 versus PC2 plot for all Q-based samples, with detailed sample names omitted for clarity. An interactive plot with sample names is available in the supporting information (Figure 23S). In this plot, the aging direction is towards the upper left quadrant.

Three main groups can be identified in this plot. The first group (circle 1 in Fig. 18) includes the field-aged PA sample of 2021 (after 7 years of field aging) and the 1 mm film of Q binder hygrothermally aged for 80 h (Q-LW80H-1). The samples are located in the upper left corner of the plot, indicating a high degree of aging. Notably, the sample subjected to 80 h of hygrothermal aging is appropriately positioned within this highly aged region. Conversely, the placement of the sample that has undergone 7 years of field aging is unexpected, raising questions about the reliability or consistency of the data for this specific sample. The second group comprises all binder films aged under different laboratory conditions (Table 2), along with some PA and SMA samples aged in both laboratory and field (from 2019 to 2023). The third group contains field-aged samples from 2014 – 2018 and mixture samples aged at 60 °C and 85 °C under 20 bar pressure, with and without humidity. Groups (2) and (3) share similar PC2 values but differ significantly in PC1. The main parameters related to this difference will be discussed in the next paragraph by analysing the loadings. In all groups, both mixture and binder film samples are present, indicating that differentiation between binder films and extracted binder samples cannot be achieved solely by PCA analysis of specific FTIR indices and rheological properties.

Fig. 19 shows the loadings on PC1 for all features. High loadings are observed for FTIR ranges of 710–734, 833–912, 984–1047, 1100–1330, 1660–1750, and 2820–2990 cm^{-1} . Rheological features such as alpha, sigma, and shift factors at 0 °C also have high loading on PC1. The differentiation between groups (2) and (3) can be effectively achieved using PC1, with the loadings of PC1 indicating that FTIR indices are highly significant. Consequently, there should be a discernible difference in the FTIR values between these groups. Notably, group (3) samples were measured using a different sample preparation method and FTIR device compared to group (2) samples. Although the carbonyl and sulfoxide values of these samples were within the normal range, PCA analysis of all FTIR indices collectively distinguished between

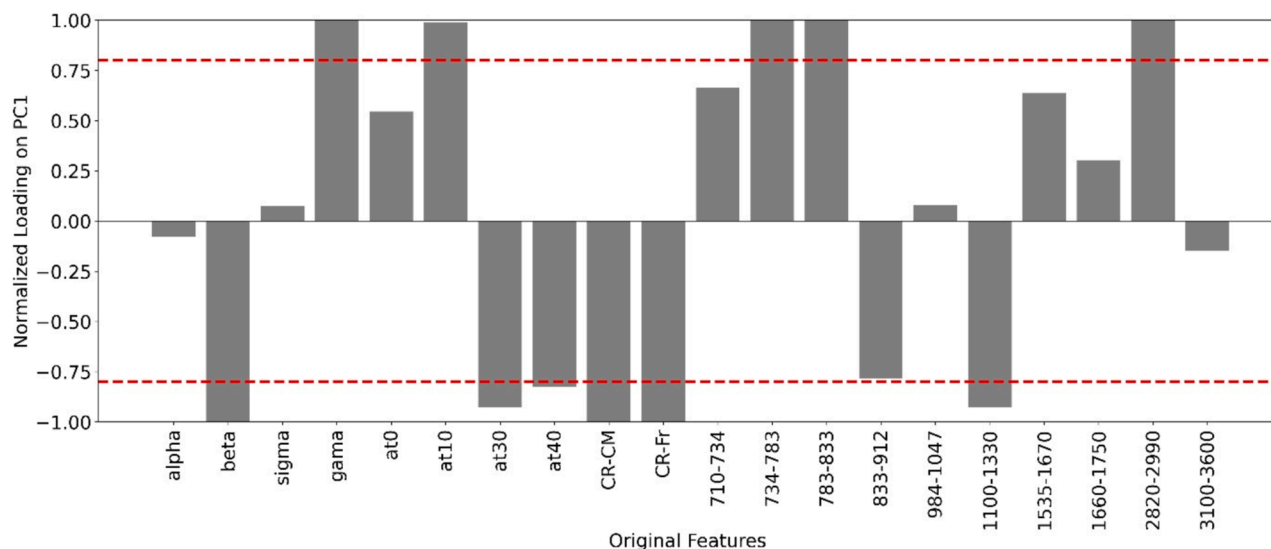


Fig. 16. Loadings of all features (FTIR + DSR parameters) for PC1. All the Q and T binder samples were used as input. A threshold of ± 0.80 was applied and marked by the orange horizontal lines to determine the significance of these loadings. (For interpretation of the references to color in this figure legend, the reader is referred to the web version of this article.)

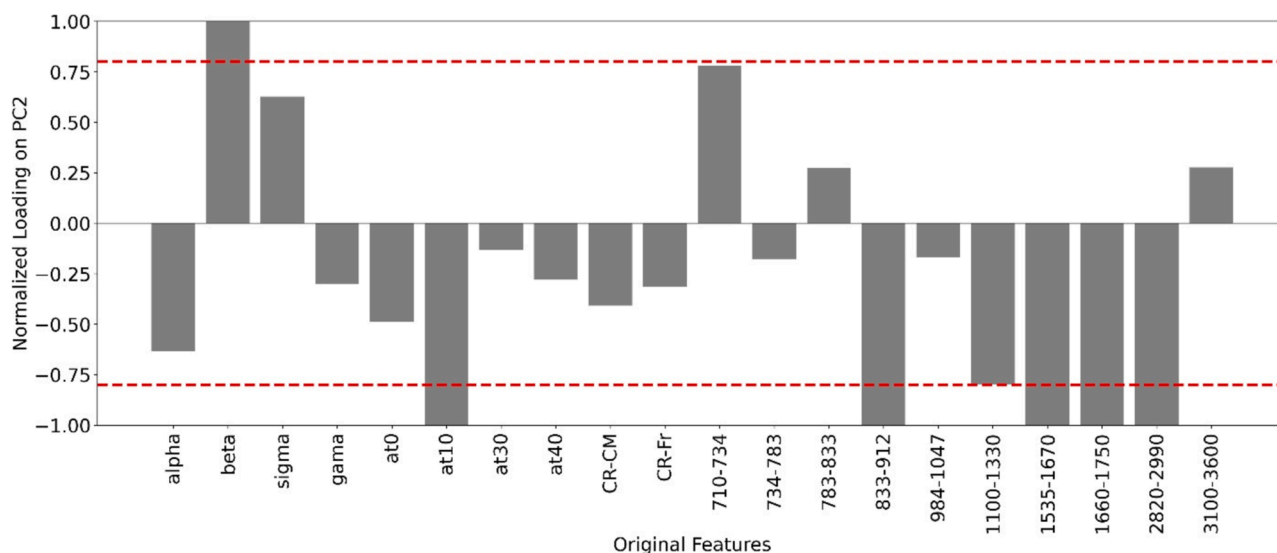


Fig. 17. Loadings of all features (FTIR + DSR parameters) on PC2. All the binder samples from both Q and T binder were used as input. A threshold of ± 0.80 was applied to determine the significance of these loadings.

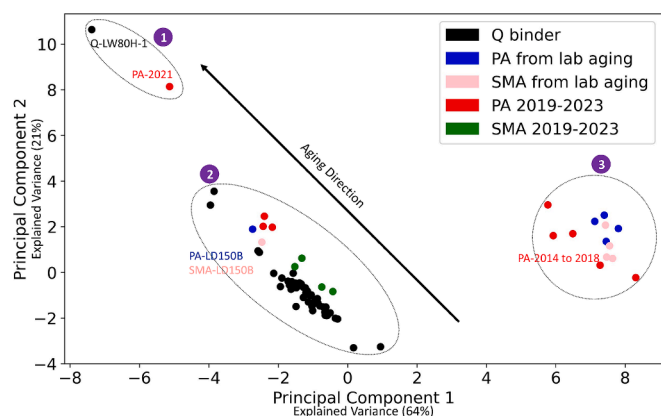


Fig. 18. PCA plot based on FTIR and DSR data for Q samples including lab-aged binder films, lab-aged mixtures, and field-aged mixtures. An interactive version of this plot, showing the exact sample names, is available in the supporting information (Figure 23S).

measurements taken by different sample preparation and devices. It is important to note that normalization, baseline correction, and indices calculation did not mask the information. For future studies, it is recommended to analyse how different sample preparations and devices affect FTIR data.

Aging, as indicated by PCA analysis, is associated not only with movement towards negative PC1 values but also towards positive PC2 values. The loadings on PC2, shown in Fig. 20, reveal that only the crossover values from rheological properties are loaded more than 80% on PC2. These loadings suggest that aging is associated with a decrease in crossover values. The PC2 component differentiates between groups (1) and (2). Given that crossover values are highly significant for PC2, differences in crossover values between Q-LW80H-1 and PA-2021 samples and group (2) samples are expected. The Q-LW80H-1 sample exhibits extremely low crossover values (Fig. 12). In contrast, the PA-2021 sample does not show unusual crossover values, indicating that further investigation is required to understand its positioning.

In summary, combining all the important features identified from both PCA analyses shows that all the features, except hydroxyl region of FTIR spectrum ($3100\text{--}3600\text{ cm}^{-1}$), are important for aging studies.

4.3.2. Chemo-rheological relationships in aging studies

In this section, the aim is to understand the relationship between chemical properties and rheological properties using all the Q-based binder, mixture, and field samples. SVR regression was used to correlate each of the rheological parameters with all the chemical parameters, and R^2 and $RMSE$ for calibration, prediction, cross-validation, and RPD are reported in Table 4S. The optimal combination of SVR parameters (C , ϵ , γ , and kernel) is presented for each rheological parameter and varies across different properties due to the unique nature of the dataset and their distinct characteristics.

The only rheological parameter with all R^2 values higher than 0.85 is the alpha parameter, which reflects the overall stiffness or viscoelastic properties of the binder. The RPD value of prediction for alpha is 3.49, which is considered to indicate excellent performance. In contrast, At40 and CR-Fr show negative R^2 and zero $RMSE$ values, indicating that the model performs worse than simply predicting the mean of the target variable. This may be due to overfitting, where the model is too complex and captures noise instead of the actual signal, resulting in poor predictions on new data. Therefore, it is concluded that the chemical properties used as features require better model development to be strongly correlated with the At40 and CR-Fr properties.

Furthermore, more details were analysed to identify the most relevant region of the FTIR spectrum for predicting alpha values. The relationship between alpha values and the index of each region of the FTIR spectrum is shown in Figure 24S with R^2 and $RMSE$ values used to compare different kernels. Specifically, Fig. 21 shows the plot of alpha values versus index values of the region $734\text{--}783\text{ cm}^{-1}$, which resulted in the highest R^2 value (0.74) and lowest $RMSE$ values (0.75). This shows that the FTIR region $734\text{--}783\text{ cm}^{-1}$ has strong predictive power for the alpha value. The chemical bonds and functional groups active in the $734\text{--}783\text{ cm}^{-1}$ range likely have a significant impact on the material's rheological behaviour, possibly due to specific interactions or structural features influencing the material's viscosity, elasticity, or other rheological properties. This region corresponds to CH bending vibrations in aromatic rings, which are indicative of rigid, multi-ring aromatic structures. These structures enhance intermolecular interactions and contribute to a more interconnected molecular network within the binder, thus affecting its viscosity and elasticity. The reduced molecular mobility resulting from these dense aromatic structures further influences the material's flow and deformation behaviour, making the $734\text{--}783\text{ cm}^{-1}$ region a strong predictor for the alpha value.

In addition to $734\text{--}783\text{ cm}^{-1}$ region, the complete range of $710\text{--}912$

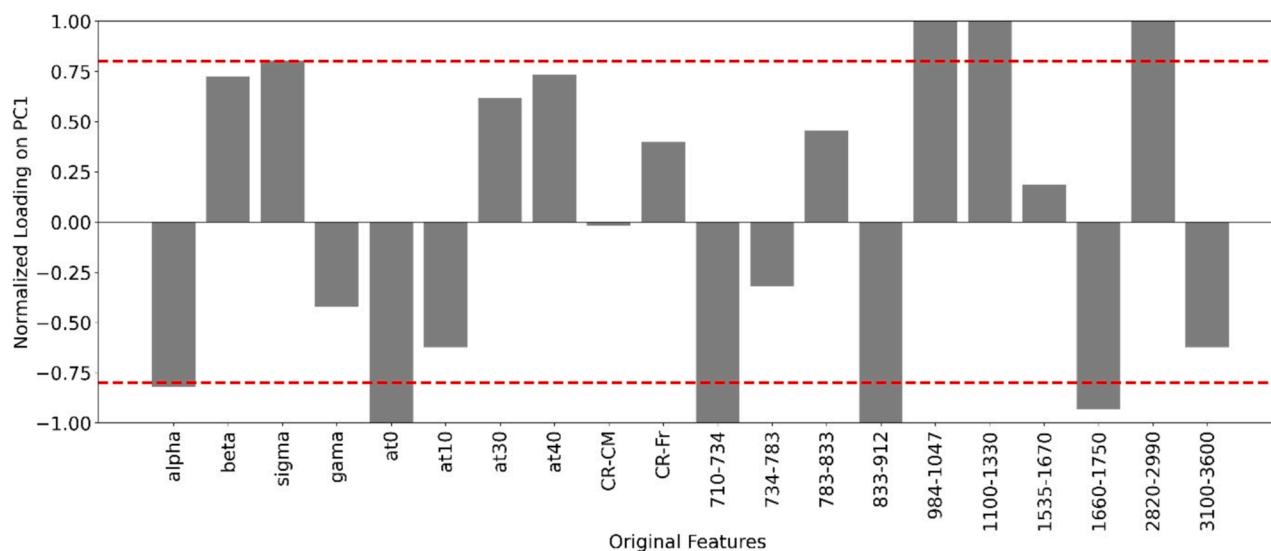


Fig. 19. Loading of all features (FTIR + DSR parameters for Q binder samples, including lab-aged binder films, lab-aged mixtures, and field-aged mixtures) on PC1. A threshold of ± 0.25 was applied to determine the significance of these loadings.

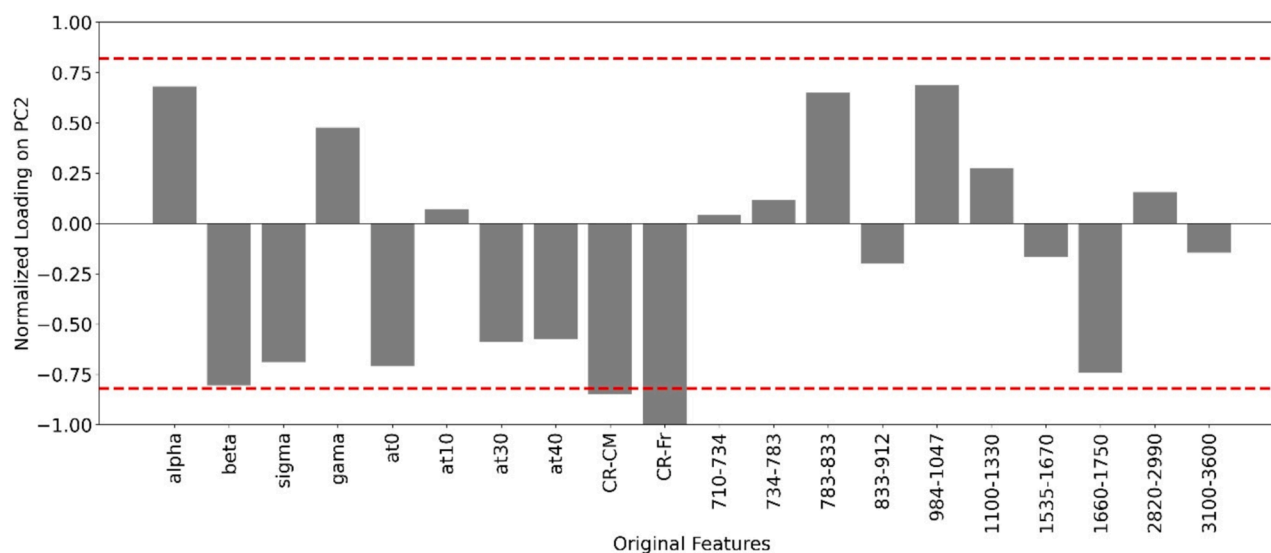


Fig. 20. Loading of all features (FTIR + DSR parameters for Q binder samples, including lab-aged binder films, lab-aged mixtures, and field-aged mixtures) on PC2. A threshold of ± 0.25 was applied to determine the significance of these loadings.

cm^{-1} also contains information on dense aromatic structures. Therefore, it is recommended to focus more on the 710–912 cm^{-1} region in FTIR analysis to gain insights into the rheological properties of materials. This can streamline analysis and reduce the complexity of data interpretation. The findings highlight the significance of the FTIR region of 710–912 cm^{-1} in predicting the alpha value, demonstrating a strong correlation and predictive capability. This region is crucial for understanding the chemical-rheological relationship and has the potential to provide a reliable basis for predictive modelling in material science.

4.3.3. Quantifying the impact of aging factors and back-calculation of field-aging conditions by MLR

This MLR analysis aims to quantify how various aging factors (i.e., temperature, pressure, and time) contribute to resulting aging in a binder and to elucidate the relationships among these factors. The trained model is then used to back-calculate the aging conditions required to achieve the same level of aging observed in field samples. A combined aging index was utilized for the MLR analysis instead of

relying solely on FTIR or DSR parameters since based on PCA analysis in section 4.3.1, almost all parameters were important for aging studies. The analysis separated lab-aged binders into hygrothermal and thermo-oxidative aging groups, expecting that the presence of humidity during aging could change the effect of other aging factors. This categorization aimed to account for the unique impacts of humidity on the aging process and binder properties. The low Pearson correlation coefficients (between ± 0.30) and VIF values of aging factors (~ 1) (Table 5S) indicated no significant multicollinearity among the input variables, justifying the appropriate use of MLR.

For the thermo-oxidative dataset, there is a discrepancy between the regression results for training data ($R^2 = 0.90$) and the Leave-One-Out Cross-Validation results ($LOOCV R^2 = -7.19$). The negative value of $LOOCV R^2$ suggests that the model might be overfitting the training data and thus performing poorly on the test data, as $LOOCV$ tests each observation based on the training results of all others. Moreover, with only 9 observations, the model is very sensitive to each individual data point. Small sample sizes can lead to unstable estimates

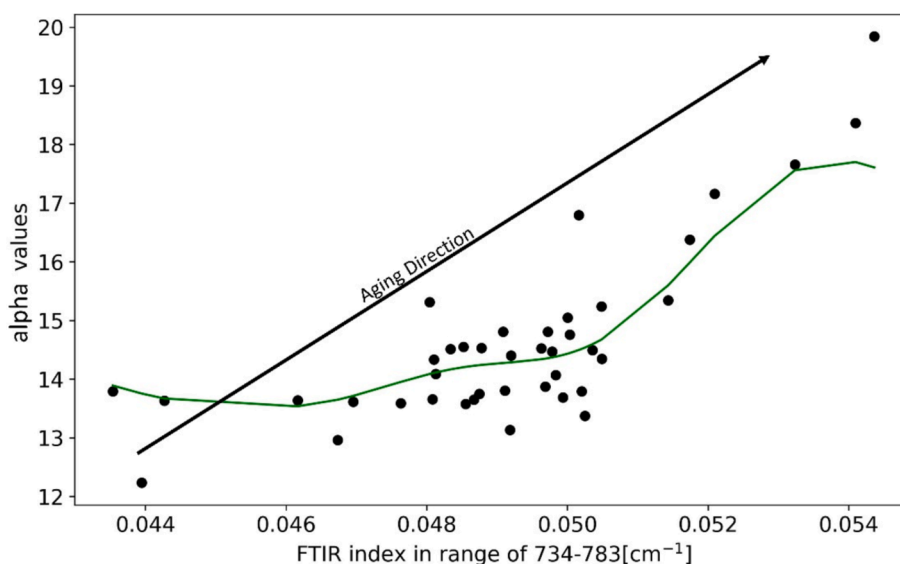


Fig. 21. Alpha from sigmoidal model versus FTIR index in range of 734–783 cm^{-1} . The green line represents the RBF-SVR model for alpha prediction versus FTIR index in the range of 734–783 cm^{-1} . (For interpretation of the references to color in this figure legend, the reader is referred to the web version of this article.)

of model performance metrics and can exaggerate the differences between training and test performance. In future works, a model for thermo-oxidative dataset should be developed using more data points.

For the hygrothermal dataset, the model had a high R-squared value for both training (0.98) cross validation ($R^2 = 0.94$) data, indicating its good performance. Despite the small sample size (10 observations), the model integrates a large proportion of the variance in the combined index. Therefore, the model of hygrothermal aged samples was selected for further investigation.

Table 4 presents the estimated coefficients for each factor. The coefficients for temperature, pressure, and time are 0.0173, 0.0266, and 0.0363 respectively. This indicates that for every unit increase in these variables, the log-transformed combined index increases by 0.0173 (p -value = 0.017), 0.0266 (p -value = 0.006), and 0.0363 (p -value < 0.001). The intercept of -4.899 represents the expected value of the log-transformed Combined index when all factors are zero, indicating a very low baseline Combined index.

The sensitivity of the combined index to aging factors can be analysed by comparing the coefficients of each factor, with higher coefficients indicating greater sensitivity. Therefore, the combined index is most sensitive to the time factor. To determine the compensatory change in one variable for a one-unit change in another, the regression model's coefficients can be used. For a one-unit change in Time ($\Delta\text{Time} = 1$), the relationships $\alpha_3 \times \Delta\text{Time} = \alpha_2 \times \Delta\text{Pressure}$ and $\alpha_3 \times \Delta\text{Time} = \alpha_1 \times \Delta\text{Temperature}$ yield $\Delta\text{Pressure} = 1.364$ and $\Delta\text{Temperature} = 2.099$. Therefore, to compensate for a one-unit change in Time, Temperature and Pressure need to change by approximately 2.099 and 1.364 units, respectively. This insight is valuable for designing future binder aging experiments.

Next, the trained MLR coefficients were used in Equation (10) to back-calculate the aging conditions that simulate nine years of field aging for porous and stone mastic asphalt. The combined indices were calculated based on the measured properties of PA-2023 and SMA-2023. The boundary conditions were set within the ranges used in this study: $60^\circ\text{C} < \text{Temperature} < 85^\circ\text{C}$, $1 \text{ bar} < \text{Pressure} < 20 \text{ bar}$, and $5 \text{ h} < \text{Time} < 40 \text{ h}$. The results indicated optimal conditions for PA-2023 as 74°C , 16 bar, and 28 h, and for SMA-2023 as 70°C , 10 bar, and 20 h. This finding suggests that the model can serve as a starting point for guiding the design of laboratory aging conditions that simulate a specific year of field aging.

It is important to note that these calculations are valid for aging of 1 mm binder films under hygrothermal aging condition. Further

investigation is required for thermo-oxidative or aqua-thermal aging conditions. Additionally, this study's limitations include the small number of data points and the exclusion of interaction terms to avoid model complexity. Future research should consider these terms with adequate data. Thus, this discussion provides a basis for future research.

4.3.4. Finding closest lab-aged sample to field aged samples by Euclidean distance

To study the similarity between field- and lab-aged samples, the Euclidean distance was calculated based on the PCA score plot (Fig. 18). For this distance calculation, field samples of PA-2023 and SMA-2023 were considered as the reference groups. The reason PA-2023 and SMA-2023 were considered as references is that these samples are the most field-aged samples, each representative of 9 years of field aging for their respective mixture types. The distances between reference samples and all other samples are presented in Table 6S in an ascending order based on distance value. The illustrative distance results are shown in Fig. 22. Q-LW20B-1 and PA-LD150B are the binder and mixture samples closest to PA-2023, while for SMA-2023, Q-LD10H-1 and SMA-LD150B are the closest binder and mixture samples, respectively.

The results based on the Euclidean distance were then compared with the MLR analysis discussed in Section 4.3.3. For PA-2023, the MLR predicts the optimal laboratory conditions as 74°C , 16 bar, and 28 h. Considering the compensatory changes in aging factors revealed by the MLR coefficients, the difference between these conditions and those of Q-LW20B-1 (closest to PA-2023 identified by Euclidean distance) is only 2.6°C , indicating that Q-LW20B-1 was aged 2.6°C cooler than necessary to precisely replicate PA-2023 properties. This consistency demonstrates the high accuracy of the identified aging conditions in replicating field samples. Similarly, the MLR-predicted laboratory conditions for SMA-2023 are 70°C , 10 bar, and 20 h, with the closest identified condition based on Euclidean distance being Q-LW5B-1 (compared with the MLR model trained based on hygrothermal conditions). The compensatory changes show a difference of 7.25°C , meaning Q-LW5B-1 was aged at 7.25°C higher temperature than required to precisely replicate SMA-2023 properties.

4.3.5. Prediction of field aging for laboratory samples using SVR

In this section, the aim is to predict the equivalence of field aging duration for each laboratory aging condition. To achieve this goal, field data were used to train an SVR model with rheological and chemical parameters as independent variables and years of field aging as the

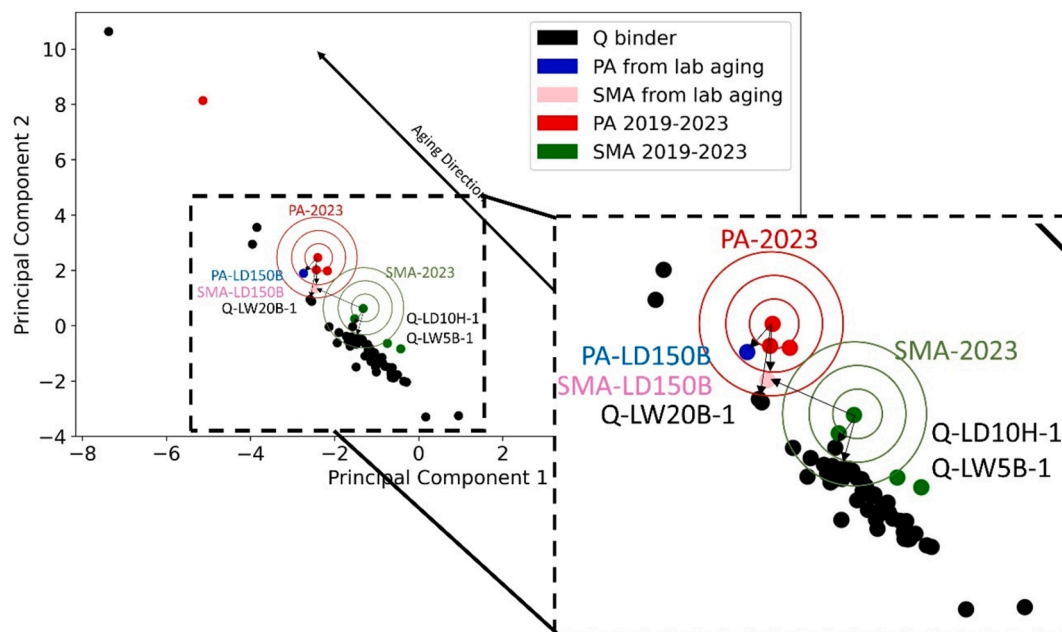


Fig. 22. Euclidean pairwise distances identifying the samples closest to PA-2023 and SMA-2023. The inset on the right provides an enlarged view of the relevant section of the PCA plot. Circles indicate the distances around each field sample.

dependent variable. Then, this model was used with properties of lab-aged samples to predict field aging years they represent. Two models were trained to evaluate their performance on different datasets: one based on SMA field data (SMA-SVR model) and the other on PA field data (PA-SVR model). The SMA-SVR model achieved an R^2 value of -0.71 and an $RMSE$ of 1.75, while the PA-SVR model achieved an R^2 value of 0.78 and an $RMSE$ of 0.91. The $RMSE$ values indicate the average magnitude of error between predicted and actual values, with lower $RMSE$ values signifying better model performance. The PA-SVR model's lower $RMSE$ (0.91) compared to the SMA-SVR model's higher $RMSE$ (1.75) suggests that it provides more accurate predictions.

The R^2 scores, however, provide additional context. The SMA-SVR model's R^2 of -0.71 implies poor fit, indicating that the model performs worse than a simple mean-based model, as it fails to capture the variability in the data effectively. In contrast, the PA-SVR model's R^2 of 0.78 demonstrates a good fit, with the model explaining a substantial portion of the variance in the data. Nonetheless, the PA-SVR model's superior R^2 and lower $RMSE$ make it the more reliable and accurate model. Consequently, the PA-SVR model was selected for further analysis in this study.

The model was evaluated using Leave-One-Out Cross-Validation (LOOCV), which showed that the SVR model with the optimized parameters ('C': 100.0, 'epsilon': 0.0001, 'gamma': 0.01, 'kernel': 'rbf') achieved a mean $RMSE$ of 0.91, indicating that the model's predictions are on average close to the actual years of field aging. The Radial Basis Function (RBF) kernel is the optimized kernel, which is well-suited for capturing non-linear relationships between the input features (rheological and chemical properties) and the output (years of field aging).

The PA-SVR model was employed to predict the equivalent years of field aging for all laboratory-aged samples, using chemical and rheological properties as inputs. Table 5 shows the most and least laboratory-aged samples with their predicted years of simulated field aging (complete table in supporting information, Table 7S), suggesting that the chemical and rheological properties of these samples are similar to those of field samples aged for approximately the predicted years indicated in the table. Given the model's $RMSE$, the true field aging of these samples is expected to be within the range of the specified year ± 0.91 years, accounting for the average prediction error and variability. Based on the predicted values, Q-LW1B-3 is the least aged sample (0.57 ± 0.91), and

Table 5

Predicted years of field aging for select lab-aged samples subjected to extreme conditions, derived from the PA-SVR model. A comprehensive table is available in the Supporting Information as Table 7S.

Sample names	predicted years of field aging ± 0.91
Q-LW1B-3	0.57
Q-LW1B-2	0.76
Q-LD60C-3	0.82
...	...
Q-LD85C-1	9.28
PA-LD150B	9.38
Q-LW85C-1	10.24
SMA-LD150B	10.46
Q-LW40H-1	10.85

Q-LW40H-1 is the most aged sample (10.85 ± 0.91). For this modelling, outlier samples such as those in clusters 1 and 3 of the PCA plot in Fig. 16 were not considered due to the sensitivity of the SVR algorithm to outliers. The predictions for both the least and most aged samples are consistent with the discussions in other sections, demonstrating the validity of the developed model. Consequently, this model is suitable for preliminary predicting the equivalent field aging of other laboratory-aged samples based on their chemical and rheological properties.

The SVR model predicts the equivalent field aging for various laboratory-aged samples, providing results that include decimal values. These decimal differences are informative, as they indicate the variation in the intensity of aging under different laboratory conditions. The conditions can be viewed as part of a continuous spectrum of aging intensities, with the decimal places representing the finer distinctions between them. For practical application, laboratory conditions should be chosen based on how closely they match the desired duration of field aging. While the predictions offer a spectrum of aging conditions, it is important to select the laboratory aging protocol that most closely corresponds to the required field aging duration. This decision should be guided by the limitations of the laboratory equipment, such as its limitation in controlling temperature, pressure, and humidity. Therefore, instead of rounding the predicted values, selecting the closest match to the target aging time will yield the most accurate results within the constraints of the available experimental setup.

It is important to acknowledge limitations of this work, particularly related to the size of the dataset used for training the SVR model. The current model is based on limited field-aged samples, which presents the potential risk of overfitting. However, this risk has been mitigated by performing additional validation, including PCA analysis and Euclidean distance comparisons between field-aged samples and lab-aged predictions. The close alignment between the model predictions and actual field data suggests that the SVR model is reasonably accurate, providing preliminary insights into field aging behaviour. A dataset with at least 30 field-aged samples would significantly improve the model's ability to generalize across different conditions. Therefore, while the current model offers valuable guidelines, the predictions should be considered preliminary until further validation with larger datasets is conducted.

5. Conclusion

This study provides a comprehensive investigation into the aging of bituminous binders under varying conditions, focusing on temperature, pressure, binder thickness, moisture, and aging duration, alongside binder sources and mixture types. The key findings are summarized as follows:

- Studying effect of aging factors on chemical and rheological properties showed that:
 - Increasing temperature, pressure, and aging duration leads to more oxidative products and significant changes in rheological properties.
 - Hygrothermal aging accelerates oxidative aging in moisture-sensitive binders.
 - Thinner binder films (1 mm) and porous asphalt samples exhibit stronger aging effects.
- The goal of categorizing samples based on binder type and aging effects was achieved using PCA.
 - PCA successfully categorized samples based on binder type and aging effects by analysing chemical (FTIR indices) and rheological properties.
 - PC1 emphasized FTIR indices and rheological parameters, while PC2 highlighted crossover values.
 - However, PCA did not distinctly separate binder films and extracted mixture samples, suggesting the need for standardizing sample preparation methods.
- To predict rheological parameters based on FTIR indices, SVR was employed.
 - The relationship between chemical properties and rheological properties was analysed by the SVR prediction model, with the alpha parameter (reflects the overall stiffness or viscoelastic properties of the binder) of sigmoidal model, reflecting overall stiffness, showing excellent predictive performance.
 - The FTIR region of 710–912 cm^{-1} was identified as critical for predicting stiffness.
 - The findings emphasize the importance of long-chain regions of FTIR spectra in future studies.
- The relationship between independent variables—temperature, pressure, and time—during the aging process of bituminous binders was assessed using MLR.
 - MLR models quantified the contributions of temperature, pressure, and time to binder aging, distinguishing between hygrothermal and thermo-oxidative aging.
 - Sensitivity analysis showed that time has the most significant impact on aging, followed by pressure and temperature.
 - To offset a one-unit change in time, temperature and pressure need to be adjusted by approximately 2 and 1 units, respectively.
 - MLR-derived coefficients were used to back-calculate optimal laboratory conditions for simulating field aging (e.g., 9 years for porous asphalt and stone mastic asphalt). The MLR model thus offers a reliable method for predicting equivalent aging conditions

and designing laboratory experiments that accurately replicate field aging.

- To identify laboratory conditions that closely resemble field samples, pairwise Euclidean distance was employed.
 - Using Euclidean pairwise distances and PA-2023 and SMA-2023 as reference points, the study identifies the laboratory aging conditions closest to the field, with Q-LW20B-1 (binder) and PA-LD150B (mixture) closest to PA-2023 and Q-LW5B-1 (binder) and SMA-LD150B (mixture) closest to SMA-2023.
 - These results underscore the effectiveness of using Euclidean distance in conjunction with predictive modelling to assess and fine-tune laboratory aging conditions to better simulate real-world aging scenarios in asphalt binders.
- The objective of estimating the duration of field aging that a laboratory sample simulates was accomplished through the application of SVR. Two SVR models were trained to establish the relationship between laboratory aging conditions and the equivalent field aging years based on PA and SMA field data separately, with the PA-SVR model demonstrating higher accuracy.
 - The Radial Basis Function (RBF) kernel effectively captures non-linear relationships between input features (rheological and chemical properties) and field aging duration.
 - A predictive model has been developed to correlate laboratory aging protocols with various field aging durations. According to the model, replicating approximately 9 years of field aging for porous asphalt can be achieved by subjecting a 1 mm film of binder to aging conditions of 85 °C, 20 bar pressure, and humidity levels exceeding 99 % for 20 h. For simulating 11 years of field aging, the recommended duration is extended to 40 h, with the temperature, pressure, and humidity conditions remaining unchanged.

This study lays a crucial foundation for future research in the field of asphalt binder aging by providing a comprehensive understanding of how various factors influence the aging process. The insights gained from the analysis of temperature, pressure, binder thickness, moisture, and aging duration not only enhance our knowledge of oxidative aging mechanisms but also provide preliminary guidelines for understanding bituminous binder aging. Future studies should focus on exploring the critical FTIR regions identified in this study, particularly the long-chain regions associated with rheological properties, could lead to more accurate predictive models for binder performance. Expanding the dataset for the MLR model will also be essential to mitigate overfitting issues and enhance its robustness. Furthermore, investigating the interplay between hygrothermal and thermo-oxidative aging in greater detail could uncover new strategies for optimizing binder formulations and aging protocols. To improve the prediction of field aging, incorporating additional field-aged samples into the training of the formulated predictive model will allow for the development of more accurate laboratory aging protocols for various field aging durations, such as 15 or 20 years. Overall, this research not only contributes valuable findings but also opens multiple avenues for further exploration, ultimately aiming to improve the durability and longevity of asphalt pavements.

CRedit authorship contribution statement

Sadaf Khalighi: Writing – review & editing, Writing – original draft, Visualization, Validation, Methodology, Investigation, Formal analysis. **Lili Ma:** Writing – review & editing, Investigation. **Yasmine Mosleh:** Writing – review & editing. **Diederik van Lent:** Writing – review & editing. **Aikaterini Varveri:** Writing – review & editing, Supervision.

Declaration of competing interest

The authors declare that they have no known competing financial interests or personal relationships that could have appeared to influence the work reported in this paper.

Acknowledgment

This paper/article is created under the research program Knowledge-based Pavement engineering (KPE, funded by Rijkswaterstaat, Netherlands with contract number 31164321). KPE is a cooperation between Rijkswaterstaat, TNO (Netherlands) and TU Delft (Netherlands) in which scientific and applied knowledge is gained about asphalt pavements and which contributes to the aim of Rijkswaterstaat to be completely climate neutral and to work according to the circular principle by 2030. The opinions expressed in this paper is solely from the authors. Data of this work will be made available on request.

Appendix A. Supplementary data

Supplementary data to this article can be found online at <https://doi.org/10.1016/j.matdes.2024.113520>.

Data availability

Data will be made available on request.

References

- J. Read, D. Whiteoak, The shell bitumen handbook. 2003: Thomas Telford.
- K. Hofer, et al., Chemical and mechanical analysis of field and laboratory aged bitumen, *Road Mater. Pavement Des.* 24 (sup1) (2023) 160–175.
- R.S. Siroma, et al., A literature review of bitumen aging: From laboratory procedures to field evaluation, *J. Test. Eval.* 50 (2) (2022) 1023–1044.
- R. Siroma, et al. A literature review of bitumen aging: from laboratory procedures to field evaluation. in *Proceedings of the RILEM International Symposium on Bituminous Materials: ISBM Lyon 2020 1*. 2022. Springer.
- J.C. Petersen, A review of the fundamentals of asphalt oxidation: chemical, physicochemical, physical property, and durability relationships, *Transp. Res. Cir.* (2009). E-C140.
- B. Hofko, M. Hospodka, Rolling thin film oven test and pressure aging vessel conditioning parameters: effect on viscoelastic behavior and binder performance grade, *Transp. Res. Rec.* 2574 (1) (2016) 111–116.
- EN 12607-1, C., 12607-1: Bitumen and Bituminous Binders—Determination of the Resistance to Hardening under Influence of Heat and Air—Part 1: RTFOT Method. European Committee for Standardization: Brussels, Belgium, 2014.
- EN 14769, C., 14769: Bitumen and Bituminous Binders—Accelerated Long-Term Ageing Conditioning by a Pressure Ageing Vessel (PAV). European Committee for Standardization: Brussels, Belgium, 2012.
- Highways, A.A.o.S. and T. Officials, Practice for short and long term ageing of hot mix asphalt. 1994, AASHTO Designation PP2.
- G.D. Airey, State of the art report on ageing test methods for bituminous pavement materials, *Int. J. Pavement Eng.* 4 (3) (2003) 165–176.
- R. Jing, et al., Laboratory and field aging effect on bitumen chemistry and rheology in porous asphalt mixture, *Transp. Res. Rec.* 2673 (3) (2019) 365–374.
- R. Jing, et al., Differences in the ageing behavior of asphalt pavements with porous and stone mastic asphalt mixtures, *Transp. Res. Rec.* 2675 (12) (2021) 1138–1149.
- R. Jing, et al. Ageing Behavior of Porous and Dense Asphalt Mixtures in the Field. in *Proceedings of the RILEM International Symposium on Bituminous Materials: ISBM Lyon 2020 1*. 2022. Springer.
- R. Jing, et al., Rheological, fatigue and relaxation properties of aged bitumen, *Int. J. Pavement Eng.* 21 (8) (2020) 1024–1033.
- Q. Qin, et al., Field aging effect on chemistry and rheology of asphalt binders and rheological predictions for field aging, *Fuel* 121 (2014) 86–94.
- P. Singhvi, et al., Impacts of field and laboratory long-term aging on asphalt binders, *Transp. Res. Rec.* 2676 (8) (2022) 336–353.
- Y. Qian, et al., Simulation of the field aging of asphalt binders in different reclaimed asphalt pavement (RAP) materials in Hong Kong through laboratory tests, *Constr. Build. Mater.* 265 (2020) 120651.
- X. Lu, Y. Talon, P. Redelius, 406-001 Aging of bituminous binders—Laboratory tests and field data. In *4th Eurasphalt Eurobitumen Congress*, 2008.
- J. Besamusca, et al., Simulating ageing of EN 12591 70/100 bitumen at laboratory conditioning compared to porous asphalt. In *5th Eurasphalt and Eurobitumen Congress*, 2012.
- J. Erskine, S. Hesp, F. Kaveh. Another look at accelerated aging of asphalt cements in the pressure aging vessel. in *Proceedings, Fifth Eurasphalt and Eurobitumen Congress*, Istanbul, Turkey. 2012.
- R. Jing, Ageing of bituminous materials, *Experimental and Numerical Characterization*. (2019).
- Climate Atlas of Canada. (n.d.) Urban Heat Island Effect. [cited 2024 11/14/2024]; Available from: <https://climateatlas.ca/urban-heat-island-effect>.
- Y. Zheng, P. Zhang, H. Liu, Correlation between pavement temperature and deflection basin form factors of asphalt pavement, *Int. J. Pavement Eng.* 20 (8) (2019) 874–883.
- J. Mirwald, et al., Impact of reactive oxygen species on bitumen aging—The Viennese binder aging method, *Constr. Build. Mater.* 257 (2020) 119495.
- D. Maschauer, et al., Viennese Aging Procedure (VAPro): Adaption for Low-Temperature Testing 1 (2020) 2022.
- F. Karim, J. Hussain, I. Hafeez, Estimating the asphalt binder film thickness using scanning electron microscope and energy dispersive X-Ray spectroscopy, *Adv. Mater. Sci. Eng.* 2021 (2021) 1–16.
- F. Karim, J. Hussain, Assessing the asphalt binder film thickness in recycled asphalt mixtures using micro-level techniques, *Materials* 14 (24) (2021) 7891.
- N. Alkofahi, T. Khedaywi, Evaluation the effect of asphalt film thickness on stripping resistance, *Int. J. Appl. Eng. Res.* 14 (2) (2019) 560–570.
- P. Lin, et al., Effects of bitumen thickness on the aging behavior of high-content polymer-modified asphalt mixture, *Polymers* 15 (10) (2023) 2325.
- S. Khalighi, et al., Exploring the significance of exposed surface area in the aging of bitumen films with equal thickness, in: *Bituminous Mixtures and Pavements VIII*, CRC Press, 2024, pp. 71–79.
- L. Ma, et al., Water diffusion mechanisms in bitumen studied through molecular dynamics simulations, *Constr. Build. Mater.* 409 (2023) 133828.
- S. Khalighi, S. Erkens, A. Varveri, Exploring the impact of humidity and water on bituminous binder aging: a multivariate analysis approach (TI CAB), *Road Mater. Pavement Des.* (2024) 1–25.
- T. López-Montero, R. Miró, Differences in cracking resistance of asphalt mixtures due to ageing and moisture damage, *Constr. Build. Mater.* 112 (2016) 299–306.
- D.J. Jacob, Heterogeneous chemistry and tropospheric ozone, *Atmos. Environ.* 34 (12–14) (2000) 2131–2159.
- C.V. Singh, et al., Formation of functionally graded hybrid composite materials with Al₂O₃ and RHA reinforcements using friction stir process, *Aust. J. Mech. Eng.* 20 (1) (2022) 141–154.
- B. Hofko, et al., Bitumen ageing—impact of reactive oxygen species, *Case Stud. Constr. Mater.* 13 (2020) e00390.
- K. Hofer, et al., Influence of selected reactive oxygen species on the long-term aging of bitumen, *Mater. Struct.* 55 (5) (2022) 133.
- S. Wu, et al., UV and thermal aging of pure bitumen—comparison between laboratory simulation and natural exposure aging, *Road Mater. Pavement Des.* 9 (sup1) (2008) 103–113.
- J. Hu, et al., Effect of ultraviolet radiation in different wavebands on bitumen, *Constr. Build. Mater.* 159 (2018) 479–485.
- A.M. da Silva Lopes, et al., Impact of aging protocols on asphalt binder behavior: a laboratory and field study, *Case Stud. Constr. Mater.* 19 (2023) e02629.
- J. Mirwald, et al., Impact of UV–Vis light on the oxidation of bitumen in correlation to solar spectral irradiance data, *Constr. Build. Mater.* 316 (2022) 125816.
- R.S. Siroma, et al., Clustering aged bitumens through multivariate statistical analyses using phase angle master curve, *Road Mater. Pavement Des.* 22 (sup1) (2021) S51–S68.
- L. Ma, et al., Chemical characterisation of bitumen type and ageing state based on FTIR spectroscopy and discriminant analysis integrated with variable selection methods, *Road Mater. Pavement Des.* (2023) 1–15.
- K. Primerano, et al., Characterization of long-term aged bitumen with FTIR spectroscopy and multivariate analysis methods, *Constr. Build. Mater.* 409 (2023) 133956.
- S. Weigel, D. Stephan, The prediction of bitumen properties based on FTIR and multivariate analysis methods, *Fuel* 208 (2017) 655–661.
- S. Weigel, D. Stephan, Bitumen characterization with Fourier transform infrared spectroscopy and multivariate evaluation: prediction of various physical and chemical parameters, *Energy Fuel* 32 (10) (2018) 10437–10442.
- L. Ma, Interactions of moisture and oxidative ageing mechanisms in paving binders: Towards improving durability of pavements. 2025.
- L. Porot, et al., Fourier-transform infrared analysis and interpretation for bituminous binders, *Road Mater. Pavement Des.* 24 (2) (2023) 462–483.
- S. Khalighi, et al., Evaluating the Impact of Data Pre-Processing Methods on Classification of Atr-Ftir Spectra of Bituminous Binders. Available at SSRN 4852406.
- R. Jing, et al., Ageing effect on chemo-mechanics of bitumen, *Road Mater. Pavement Des.* 22 (5) (2021) 1044–1059.
- 14770, E., Bitumen and bituminous binders—Determination of complex shear modulus and phase angle using a Dynamic Shear Rheometer (DSR). 2012, European Committee for Standardization Brussels.
- N.I.M. Yusoff, et al., Modelling the rheological properties of bituminous binders using mathematical equations, *Constr. Build. Mater.* 40 (2013) 174–188.
- G. Rowe, G. Baumgardner, M. Sharrock, Functional forms for master curve analysis of bituminous materials, in *Advanced testing and characterization of bituminous materials*, two volume set. 2009, CRC Press. p. 97-108.
- M. Domazet-Lošo, B. Haubold, Efficient estimation of pairwise distances between genomes, *Bioinformatics* 25 (24) (2009) 3221–3227.
- B. Schölkopf, A. Smola, Support vector machines and kernel algorithms, in: *Encyclopedia of Biostatistics*, Wiley, 2005, pp. 5328–5335.
- R.K. Douglas, et al., Rapid prediction of total petroleum hydrocarbons concentration in contaminated soil using vis-NIR spectroscopy and regression techniques, *Sci. Total Environ.* 616 (2018) 147–155.
- B. Hofko, et al., Repeatability and sensitivity of FTIR ATR spectral analysis methods for bituminous binders, *Mater. Struct.* 50 (2017) 1–15.
- S. Ren, et al., Toward the long-term aging influence and novel reaction kinetics models of bitumen, *Int. J. Pavement Eng.* (2022) 1–16.

- [59] F. Liu, et al., On the linking of the rheological properties of asphalt binders exposed to oven aging and PAV aging, *Int. J. Pavement Eng.* 22 (3) (2021) 331–340.
- [60] M. Scarsella, et al., Petroleum heavy ends stability: evolution of residues macrostructure by aging, *Energy Fuel* 13 (3) (1999) 739–747.
- [61] Y. AbuHassan, et al., Effect of extraction solvents on rheological properties of recovered asphalt binders, *Journal of Transportation Engineering, Part B: Pavements* 145 (1) (2019) 04018064.